Homeodomain protein Sxi1α independently controls cell-cell fusion and gene expression during sexual reproduction in *Cryptococcus deneoformans*

Jun Huang, Anna E. Lehmann, Patricia P. Peterson, Ziyan Xu, Liping Xiong, Sheng Sun, and Joseph Heitman*

Department of Molecular Genetics and Microbiology, Duke University Medical Center, Durham, NC 27710, USA

* Corresponding author: Joseph Heitman
Email: heitm001@duke.edu

Keywords: Homeodomain protein; Sexual reproduction; Cell fusion; Transcriptional regulation.

Abstract

Sex-specific homeodomain (HD) proteins are key regulators of cell identity and sexual development in fungi, typically functioning as heterodimers to govern transcription. In the human fungal pathogens *Cryptococcus neoformans* and *Cryptococcus deneoformans*, the HD proteins Sxi1α and Sxi2**a** (Sex-inducer 1α and 2**a**) have been characterized as interacting components that play critical roles in sexual development during α x **a** sexual reproduction. α cells are the predominant mating type in natural populations of *Cryptococcus*, and unisexual (same-sex) mating can also occur in certain genetic backgrounds. The roles of Sxi1α and Sxi2**a** in unisexual reproduction are not fully understood. To elucidate the functions of Sxi1α and Sxi2**a** in unisexual reproduction and downstream transcriptional regulation, we first applied AlphaFold3 to predict their structures, which revealed the potential for both heterodimeric and homodimeric complexes. We subsequently deleted *SXI1*α and *SXI2***a** in the hyper-filamentous self-fertile *C. deneoformans* strains XL280α and XL280**a**. Disruption of these genes did not result in noticeable defects in vegetative growth, virulence-associated traits, colony morphology, sporulation, or competitiveness during unisexual crosses. Interestingly, both bilateral (mutant x mutant) and unilateral (mutant x wildtype) crosses involving the *sxi1*αΔ mutant significantly increased α-α cell fusion efficiency, suggesting a previously unrecognized inhibitory role for Sxi1α in regulating same-sex cell fusion. Transcriptomic analysis of *sxi1*αΔ and *sxi2***a**Δ mutants led to the identification of unique subsets of genes negatively regulated by each transcription factor during unisexual reproduction. Additionally, α x **a** crosses between deletion mutants for *SXI1*α, *SXI2***a**, or both revealed differential regulation of mating-type (*MAT*) loci genes dependent only on *SXI1*α or *SXI2***a**. Together, our findings revealed an unexpected function of Sxi1α in regulating cell fusion, highlighting the versatile roles of HD transcription factors in fungal sexual reproduction. Additionally, our data suggest that *SXI1*α and *SXI2***a** have distinct regulatory roles in both unisexual and α x **a** sexual reproduction and may function as homodimeric complexes to exert opposing regulatory effects on sex-specific *MAT* genes.

Author Summary

Like many eukaryotic organisms, fungal sexual reproduction reshuffles genetic material, producing novel genetic variants with increased fitness and/or adaptive potential. The human fungal pathogen *Cryptococcus deneoformans* is widespread in the environment and can cause severe infections in immunocompromised individuals. This species reproduces between cells of either opposite mating types (α-**a** mating) or the same mating type (α-α and **a**-**a** unisexual reproduction). The mating type-specific homeodomain transcription factors Sxi1α and Sxi2**a** are known to form a complex that broadly controls sexual development upon α and **a** cell fusion. Here, we found Sxi1α inhibits cell fusion during unisexual reproduction, while its usual partner, Sxi2**a**, shows only limited inhibition in certain genetic contexts. Further, we show that Sxi1α and Sxi2**a** regulate the transcription of distinct gene sets during both α-**a** and unisexual reproduction, including many within the mating-type (*MAT*) loci, and often act in opposing manners. Together, these findings reveal that Sxi1α and Sxi2**a** function both collectively and independently, thereby generating a more flexible and fine-tuned mating control system than previously recognized and advancing our understanding of how this organism produces genetic variation and adapts to changing environments.

83 **Introduction**

84 Sexual reproduction is a key process in eukaryotic organisms, promoting genetic diversity and
85 facilitating adaptation to changing environments. In fungi, this process is controlled by the mating-type
86 (*MAT*) locus, a specific genomic region containing genes required for successful mating [1]. Among these
87 genes, pheromone and pheromone receptors (P/R) are involved in signal transduction and recognition
88 between mating partners, and homeodomain (HD) transcription factors act as master regulators that control
89 the expression of genes necessary for sexual development [2,3]. In the model yeast *Saccharomyces*
90 *cerevisiae*, **a**1 and α2 are well-characterized HD proteins, forming **a**1-α2 heterodimers that bind DNA
91 cooperatively to repress transcription of cell type-specific genes [4,5]. Unlike **a**1, which has no known role
92 in the absence of α2, α2 can form homodimers with no established function, as well as partner with the
93 Mcm1 cofactor to repress **a**-specific genes in α and **a**/α cells [6–9]. In the corn smut fungus *Ustilago maydis*,
94 the HD proteins bWest (bW) and bEast (bE) dimerize to regulate fungal morphological switching and
95 interactions with the plant host [10–13]. Similarly, sexual development in the mushroom *Coprinus cinereus*
96 requires the physical interaction of two HD proteins, HD1 and HD2 [14]. Conserved and convergent
97 functionality of HD transcription factors across diverse fungi illustrates their centrality to species survival
98 and proliferation.

99 The human fungal pathogen *Cryptococcus neoformans* is the predominant cause of cryptococcal
100 meningoencephalitis worldwide, whereas its sister species *C. deneoformans* displays a more
101 geographically restricted distribution and is more frequently encountered in certain regions, particularly in
102 Europe [15–17]. Interestingly, in *C. neoformans* and *C. deneoformans*, the *P/R* and *HD* genes as well as
103 additional genes reside in a relatively large (>100 kb) *MAT* locus [2,17–19]. In addition to its direct role in
104 α x **a** sexual reproduction, the *MAT* locus is associated with several other functions in *Cryptococcus*,
105 including virulence and uniparental mitochondrial inheritance (mito-UPI), in which mitochondrial DNA is
106 predominantly inherited from the *MAT***a** parent after α x **a** sexual reproduction [20,21]. We previously
107 identified the *Cryptococcus* sex-specific HD proteins Sxi1α (Sex inducer 1α) and Sxi2**a** (Sex inducer 2**a**),
108 which heterodimerize upon α-**a** cell fusion and are involved in key development processes including cell
109 identify determination, sexual development, and mito-UPI [2,21,21–25]. Our group and others have
110 identified several Sxi1α-Sxi2**a** targets for which proper temporal expression is essential for sexual

111 development. For example, *CPR2* (*Cryptococcus* pheromone receptor 2) governs α-**a** cell fusion, and *CLP1*
112 (clampless 1) is required for post-cell fusion dikaryotic filament formation [26–29].

113 In addition to α-**a** sexual reproduction, unisexual reproduction can also occur between partners of
114 the same mating type (mainly α x α) in *C. neoformans* and *C. deneoformans* [30–32]. In natural
115 *Cryptococcus* populations, *MAT*α isolates are predominant among both clinical and environmental samples,
116 suggesting that α x **a** heterothallic sexual reproduction is infrequent [20,33], even though population
117 genomics studies have shown that recombination is occurring among *Cryptococcus* isolates in nature
118 [33,34]. This strong bias in *MAT* locus distribution may, at least in part, be explained by the occurrence of
119 unisexual reproduction, which enables genetic recombination and propagation in the absence of a
120 compatible mating partner [30,35,36]. As key sex-specific transcriptional regulators, the roles of Sxi1α and
121 Sxi2**a** in unisexual reproduction and their transcriptional targets remained to be elucidated.

122 In this study, we sought to determine whether Sxi1α and Sxi2**a** are involved in same-sex mating in
123 *C. deneoformans*. AlphaFold3 structural prediction suggested that Sxi1α and Sxi2**a** may form both
124 heterodimer and homodimer complexes. Taking advantage of the hyper-filamentous *C. deneoformans*
125 congenic isolates XL280α and XL280**a** [37], along with a CRISPR/Cas9-based gene editing system [38,39],
126 we deleted *SXI1*α and *SXI2***a** in XL280α and XL280**a**, respectively. Consistent with previous results, we
127 found that *SXI1*α and *SXI2***a** are dispensable for vegetative growth and multiple virulence factors, including
128 thermotolerance at 37°C, polysaccharide capsule formation, and melanin production. Interestingly, crosses
129 with the *sxi1α*Δ mutants, either unilateral or bilateral, led to a significant increase in α-α fusion efficiency. A
130 similar enhancement was observed in unilateral *sxi2***a**Δ crosses during **a**-**a** fusion, while bilateral crosses
131 between *sxi2***a**Δ mutants showed no such effect, pointing to a previously unrecognized inhibitory function
132 of Sxi1α in same-sex cell fusion. No obvious defects in colony morphology, hyphal development, basidium
133 formation, sporulation, spore germination, or competitiveness were detected in *sxi1*αΔ or *sxi2***a**Δ mutants
134 during unisexual reproduction. Transcriptomic analysis revealed distinct sets of genes for which expression
135 differences are regulated only by Sxi1α, independent of its canonical interacting partner Sxi2**a**. The Sxi1α-
136 dependent gene set in the unisexual crosses is markedly smaller and has limited overlap with that in α x **a**
137 crosses, further supporting the hypothesis that Sxi1α has distinct, Sxi2**a**-independent functions in these
138 different reproductive modes.

139 Our results suggest a novel function of Sxi1α in regulating cell-cell fusion, expanding our
140 understanding of how HD proteins contribute to fungal sexual reproduction. Additionally, we show that
141 Sxi1α and Sxi2**a** have transcriptional regulatory effects both dependent upon and independent of one
142 another, evidence that when coupled with our structural predictions supports the hypothesis that Sxi1α may
143 have distinct functions as both a heterodimer and as a homodimer analogous to α2 in the budding yeast.
144 Overall, these findings further our understanding of how sexual reproduction is regulated in this important
145 human fungal pathogen and reveal important differences in Sxi1α transcription factor activity between
146 unisexual and α-**a** sexual reproduction.

Results

Sxi1α **and Sxi2a are predicted to form a heterodimer**

To study the impact of the homeodomain proteins Sxi1α and Sxi2**a** on unisexual reproduction in *Cryptococcus*, we selected to study XL280α and XL280**a**, a pair of congenic *C. deneoformans* strains, that are well-known for their ability to undergo unisexual reproduction involving robust self-filamentation and sporulation [30,37]. Sxi1α and Sxi2**a** are conserved between *C. neoformans* and *C. deneoformans*, and homeodomain (Pfam:00046) or homeobox KN domains (from **KN**OX family transcription factors, Pfam:PF05920) were found within the sequences via an NCBI conserved domain search (Fig 1A). Both domains are structurally related, sharing DNA-binding functions through a helix-turn-helix motif, consistent with potential functional relevance in governing gene expression. Similar to our previous report with yeast two-hybrid analysis [2,22], a heterodimer between Sxi1α and Sxi2**a** was predicted by AlphaFold3 protein-protein complex prediction (Fig 1B). Pairwise structural alignments between the predicted Sxi1α-Sxi2**a** heterodimer and the crystal structure of the *S. cerevisiae* **a**1-α2 heterodimer [40] revealed robust structural similarity between the two homeodomain complexes with an RMSD value of 0.561 angstroms between 49 pruned atom pairs (Fig 1C). Similarly, the Sxi1α-Sxi2**a** heterodimer exhibited high structural similarity to the AlphaFold3-predicted bW-bE heterodimer from the corn smut fungus *Ustilago maydis*, with a RMSD of 1.069 angstroms across 40 pruned atom pairs, supporting a conserved structure for the *MAT* locus-specific HD complex in fungi.

Previous studies showed that, in addition to forming a heterodimer with **a**1, *S. cerevisiae* α2 forms a homodimer to repress **a**-specific genes [9]. To determine whether Sxi1α and Sxi2**a** might also form homodimers, we utilized AlphaFold3 to model Sxi1α-Sxi1α and Sxi2**a**-Sxi2**a** interactions. The predictions indicated potential low-confidence homodimer formation for Sxi1α-Sxi1α (ipTM = 0.14, pTM = 0.23) and Sxi2**a**-Sxi2**a** (ipTM = 0.20, pTM = 0.24) (Fig 1D). These low interface and predicted TM-scores suggest weak or unstable interactions, and further experimental validation is needed to determine their biological relevance.

175 **Sxi1α and Sxi2a are dispensable for *in vitro* growth and virulence-related traits**

176 To further characterize the phenotypic impact of Sxi1α and Sxi2**a**, we deleted the *SXI1*α and *SXI2***a**
177 genes in XL280α and XL280**a**, respectively, with a CRISPR/Cas9-based strategy. In combination with a
178 previously established TRACE electroporation protocol [38,39], multiple independent drug-resistant
179 transformants [4 for XL280α *sxi1*αΔ::*NAT* and 2 for XL280**a** *sxi2***a**Δ::*NEO*] were constructed and confirmed
180 with correct genotypes as deletion mutants based on 5' junction, 3' junction, and internal ORF-specific PCR
181 analysis (Fig 2A). Mapping of reads generated from Illumina whole-genome sequencing further confirmed
182 the complete deletion of the genes in all four *sxi1*αΔ mutants and one of the two *sxi2***a**Δ mutants, and a
183 partial gene deletion in the other *sxi2***a**Δ mutant (Fig 2B). Interestingly, in some of the mutants elevated
184 read-depths were observed in the flanking regions employed for homologous recombination during gene
185 deletion, indicating potential concatemeric or ectopic insertions [41] of the resistance cassette (Fig 2B).

186 We next performed competition assays to assess the impact of Sxi1α and Sxi2**a** on fungal fitness
187 during vegetative growth. Equal amounts of mutant and wildtype cells were used to inoculate in liquid YPD
188 medium and sampled at the beginning (0h), as well as after 24h and 48h of incubation at 30°C, to assess
189 the population dynamics. In all cases, the *sxi1*αΔ and *sxi2***a**Δ deletion strains maintained their proportion
190 in the culture with respective to the co-culturing wildtype strain, suggesting the mutations confer no
191 detectable fitness defect (Fig 2C). Additionally, we characterized the contributions of Sxi1α and Sxi2**a** to
192 several major virulence traits: thermotolerance at 37°C, capsule formation, and melanin production.
193 Consistent with our previous reports in *C. neoformans* [23], none of the *sxi1*αΔ or *sxi2***a**Δ *C. deneoformans*
194 deletion strains displayed altered virulence traits compared to the XL280 wildtype strains (Fig 2D-2F).
195 Taken together, these results indicate that the loss of *SXI1*α and *SXI2***a** does not affect the fitness of the
196 XL280 strain during vegetative growth and has no impact on virulence-related traits under the conditions
197 tested.

198

199 **Sxi1α and Sxi2a are dispensable for morphology, sporulation, and cell viability during unisexual**
200 **reproduction**

201 We next investigated whether Sxi1α and Sxi2**a** are involved in unisexual reproduction in the XL280
202 background. When grown on mating and selfing inducing MS solid medium [42] as solo-cultures, all of the

203 tested *sxi1*α∆ and *sxi2***a**∆ mutants were able to produce elongated hyphae as well as basidia and
204 basidiospore chains at levels similar to the XL280 wildtype controls (Fig 3A and 3B), with no discernable
205 differences in the basidia and basidiospores observed by scanning electron microscope (SEM) (Fig 3C).
206 Thus, the deletion of *SXI1*α and *SXI2***a** did not affect unisexual reproduction morphologically in the XL280
207 background. Additionally, we collected random meiotic basidiospores by microdissection to test the effect
208 of Sxi1α and Sxi2**a** on spore germination rates and cell viability and found no significant difference in
209 germination rates between spores produced by the *sxi1*α∆ mutants and XL280α (p-values: 0.682 (*sxi1*α∆#4
210 vs XL280α) and 0.125 (*sxi1*α∆#5 vs XL280α), Welch's t-test), as well as between spores produced by the
211 *sxi2***a**∆ mutants and XL280**a** (p-values: 0.591 (*sxi2***a**∆#6 vs XL280**a**:) and 0.750 (*sxi2***a**∆ #7 vs XL280**a**),
212 Welch's t-test) (Fig 3D). No significant difference in spore germination rate was observed between the
213 congenic wildtype strains XL280α and XL280a (p-value: 0.0856, Welch's t-test) (Fig 3D).
214 We previously observed that strains capable of undergoing unisexual reproduction exhibit higher
215 competitiveness than mutants with unisexual reproduction defects, attributable to enhanced hyphal growth
216 and sporulation [43]. To assess the effects of *SXI1*α and *SXI2***a** deletion on this metric of unisexual
217 reproduction efficiency, for each deletion strain we mixed equal numbers of cells from the mutant (containing
218 a dominant drug-resistant marker) and its wildtype control strain (sensitive to drug), and spotted the mixture
219 on MS medium to induce unisexual reproduction. After robust sporulation was observed (i.e., ~10 days
220 post plating), we dissected two populations: 1) random basidiospores from the periphery where sporulation
221 occurs, and 2) the center of the spot where cells remain mostly as yeast (Fig 3E, left panel). Germinated
222 dissected spores/yeast cells were transferred onto YPD plates containing selective drug (i.e., NAT or NEO)
223 to determine from which strain in the mixture they originated from. For both *sxi1*α∆ and *sxi2***a**∆, the ratios
224 between mutant and wildtype among the basidiospores at the periphery were similar to those among the
225 yeast cells at the center (spores/yeast, p-values: 0.5398275 (*sxi1*α∆) and 0.379667 (*sxi2***a**∆), paired t-test),
226 indicating the loss of Sxi1α and Sxi2**a** did not affect fungal competitiveness during unisexual reproduction
227 (Fig 3E, right panel).
228
229
230

231 **Sxi1α is critical for unisexual cell-cell fusion**

232 In the presence of a helper strain serving as a pheromone donor, α x α and **a** x **a** outcrossing can
233 be facilitated in *C. deneoformans* in so-called Ménage à trois matings [22,30] (Fig 4A). Previously, our
234 results from α x **a** sexual reproduction suggested that Sxi1α and Sxi2**a** function after cell-cell fusion [2].
235 Although cell-cell fusion is dispensable for solo unisexual reproduction, it may still occur under certain
236 conditions, such as during α x α outcrossing [22,30]. Given the limited understanding of the role of Sxi1α
237 in this context, we sought to determine whether Sxi1α is involved in cell-cell fusion during α x α outcrossing.
238 In the presence of a donor strain (JEC20, *MAT***a** *NAT*^{S} *NEO*^{S}), equal numbers of cells from strains XL280α
239 and *sxi1*αΔ that were differentially resistant to *NAT* and *NEO* were mixed (*SXI1*α x *sxi1*αΔ, *SXI1*α x *sxi1*αΔ,
240 and *sxi1*αΔ x *sxi1*αΔ) and spotted on V8 agar (pH=7.0) to induce sexual reproduction. After 72 hours of
241 incubation, cells were collected. The fusion frequency was fewer than 5.04×10^{-8} in two independent sets
242 of the XL280α *NAT* x XL280α *NEO* crosses, with fusion products identified by screening colonies for NAT
243 and NEO resistance. In contrast, significantly higher fusion frequencies were found in *sxi1*αΔ::*NAT* x
244 *sxi1*αΔ::*NEO* (22.5-fold higher than wildtype, frequency: 1.13×10^{-6}, p-value: 0.0013, Welch's t-test) and
245 *sxi1*αΔ::*NAT* x XL280α *NEO* (62.9-fold higher than wildtype, frequency: 3.17×10^{-6}, p-value: 0.0288, Welch's
246 t-test) (Fig 4B). Taken together, these findings demonstrate that cell-cell fusion between *MAT*α cells is
247 significantly increased when the *SXI1*α gene is deleted in at least one of the two strains.

248 We then asked whether Sxi2**a** has a similar effect on cell-cell fusion during **a** x **a** unisexual mating
249 (Fig 4A). Interestingly, with the presence of a donor strain (JEC21, *MAT*α, *NAT*^{S} *NEO*^{S}), the fusion
250 frequency between XL280**a** *NAT* and XL280**a** *NEO* was 2.43×10^{-6}, while no significant difference in fusion
251 frequency was found in *sxi2***a**Δ::*NAT* x *sxi2***a**Δ::*NEO* (20% of the wildtype, frequency 5.43×10^{-7}, p-value:
252 0.1204, Welch's t-test). In contrast, the fusion frequencies between *sxi2***a**Δ::*NAT* x XL280**a** *NEO* (7.2-fold
253 higher than wildtype, frequency 1.79×10^{-5}, p-value: 0.0086, Welch's t-test), XL280**a** *NAT* x *sxi2***a**Δ::*NEO*
254 (4.6-fold higher than wildtype, frequency 1.13×10^{-5}, p-value: 0.0002, Welch's t-test) were significantly higher
255 than the wildtype cross (Fig 4C).

256 We hypothesized that NAT and NEO resistant colonies, carrying both selectable markers after cell-
257 cell fusion event, would exhibit diploid DNA content, or triploid if the fusion involved a non-selective donor
258 strain (Fig 4A). To verify the ploidy of fusion products from α x α and **a** x **a** outcrosses, flow cytometry

259 analysis was performed. With *C. neoformans* haploid strain H99 and diploid strain CnLC6683 as controls
260 [44], all NAT- or NEO- containing outcrossing parent strains were confirmed to possess haploid DNA content
261 (Fig 4D). Two independent NAT and NEO resistant colonies from Ménage à trois matings were randomly
262 selected for analysis. As expected in the α x α fusion assay, diploid DNA content was observed in bilateral
263 crosses between *sxi1*αΔ deletion mutants. In contrast, haploid DNA content was detected in XL280α *NAT*
264 x XL280α *NEO* and *sxi1*αΔ::*NAT* x XL280α *NEO* crosses. The presence of haploid NAT and NEO resistant
265 colonies suggests that our assay may slightly overestimate the true frequency of cell-cell fusion events,
266 likely due to genome recombination during unisexual reproduction. Similarly, in **a** x **a** crosses, FACS
267 analysis revealed diploid DNA content in fusion products from XL280**a** *NAT* x XL280**a** *NEO*, *sxi2***a**Δ::*NAT* x
268 *sxi2***a**Δ::*NEO*, and XL280**a** *NAT* x *sxi2***a**Δ::*NEO*, whereas haploid DNA content was found in the *sxi2***a**Δ::*NAT*
269 x XL280**a** *NEO* cross (Fig 4D). To further confirm whether the donor cell directly participated in fusion
270 events, genotyping PCR was performed to amplify *STE20***a** and *STE20*α, allelic variants of the same
271 mating-type-specific genes located with the *MAT* locus. None of the independent fusion products contained
272 the *STE20* allele from the pheromone donor's mating type, indicating that any triploid products involving
273 the donor strain are rare and were not observed in our analysis (Fig 4D and 4E).
274
275 **Sxi1α and Sxi2a regulate expression of unique subsets of genes in unisexual crosses**
276 To further explore potential roles for Sxi1α and Sxi2**a** in unisexual and α x **a** sexual reproduction,
277 we performed RNA-sequencing (RNA-seq) of solo-cultures (XL280α, XL280**a**, *sxi1*αΔ, and *sxi2***a**Δ), and
278 co-cultures including a wildtype cross (XL280α x XL280**a**), unilateral crosses (*sxi1*αΔ x XL280**a** and XL280α
279 x *sxi2***a**Δ), and a bilateral mutant cross (*sxi1*αΔ x *sxi2***a**Δ). Reads were mapped to a concatenated assembly
280 consisting of a chromosome-level XL280α genome and the XL280**a** *MAT***a** locus [45], with *MAT**a***- or *MAT*α-
281 masked versions used for solo-cultures and the unmasked assembly for co-cultures. We acquired a mean
282 of 22.4 M reads per sample (SD = 7.6 M) and achieved a mean alignment rate of 95.2% (SD = 0.8%).
283 Genes with at least 1 TPM in at least one sample were retained for downstream analysis. In both α and **a**
284 solo-cultures, principal component analysis (PCA) of the 500 most variable transcripts showed that *SXI1*α
285 or *SXI2***a** presence/absence explained the majority of the variance (S1A and S1B Fig). One replicate of
286 *sxi1*αΔ clustered separately from the others in both principal component space and in hierarchical clustering

287 of the relative (scaled vst normalized) expression of the top 500 most variable genes (S1C Fig). Therefore,
288 this replicate was excluded from downstream expression analysis. Re-analysis without this replicate
289 resulted in tighter clustering of replicates and a larger proportion of variance explained by PC1 (S1D Fig).
290 All four co-culture crosses showed clear clustering of technical replicates and separation by genotype (S1E
291 Fig). PC1 (62% variance) is seemingly explained by the presence of a functional copy of both *SXI1*α and
292 *SXI2***a** versus crosses where one or both genes were deleted. Interestingly, PC2 (25%) shows strong,
293 discrete clustering by genotype, indicating transcriptional differences between crosses lacking *SXI1*α,
294 *SXI2***a**, and both *SXI1*α and *SXI2***a** (S1E Fig).

295 Differential expression analysis was performed with DESeq2. In all comparisons, genes with p_{adj}
296 $\leqslant 0.05$ and $|\log_2 FC| \geqslant 1$ were treated as differentially expressed (DEGs). In the *sxi1*αΔ comparison, *SXI1*α
297 was identified as a DEG, and further analysis of the mapped RNA-seq reads showed that they were
298 concentrated at the same regions with a high rate of mapping of the Illumina DNA-seq reads (S2 Fig and
299 Fig 2B). No reads were detected in the open reading frame. This suggests that the 5' UTR region used for
300 homologous recombination may have integrated ectopically in the genome and/or increased in copy number.
301 A *MAT*α-adjacent gene, *FAO1*, was also identified as a DEG in the *sxi1*αΔ solo culture. Reads mapping to
302 this gene were concentrated at the 3' end that was also part of the homology region used for integration of
303 the selectable marker during *SXI1*α gene deletion. It is therefore likely that this effect is also an artifact of
304 ectopic integration of the resistance cassette. Based on these observations, *SXI1*α, *FAO1*, and *SXI2***a** are
305 excluded from consideration as DEGs.

306 In solo-cultures, *sxi1*αΔ had 19 DEGs compared to XL280α, while *sxi2***a**Δ had 23 DEGs relative to
307 XL280**a** (Fig 5A, 5B and TableS1). There were no shared DEGs between *sxi1*αΔ and *sxi2***a**Δ, underscoring
308 the potential that Sxi1α and Sxi2**a** may have distinct, nonoverlapping roles during unisexual reproduction
309 (Fig 5C). Notably, Amt2 (CNJ01880) [46], homologous to a well-characterized ammonium permease
310 required for mating under low-nitrogen conditions in *C. neoformans*, was upregulated in the *sxi1*αΔ mutant.
311 Gene ontology (GO) enrichment analysis of the identified DEGs in *sxi1*αΔ revealed two significantly
312 enriched terms, *nucleobase transport* and *transmembrane transport* (S3A Fig), whereas no significant
313 enrichment was observed for DEGs from the *sxi2***a**Δ mutant.
314

315 ***SXI1*α and *SXI2*a have distinct and overlapping transcriptional effects in unisexual and α-a sexual**
316 **crosses**

317 Given the apparent α- and **a**- specific transcriptional roles of *SXI1*α and *SXI2***a** during unisexual
318 reproduction, we next questioned whether these transcription factors may also function independently of
319 one another, in addition to their known function as a heterodimer, during α x **a** sexual reproduction. We
320 compared transcriptional changes in α x **a** crosses of opposite mating type XL280 parents deficient for one
321 (unilateral cross) or both (bilateral cross) transcription factors. Comparing all mutant crosses to the wildtype
322 cross XL280α x XL280**a**, we identified 336, 190, and 202 DEGs in *sxi1*αΔ x XL280**a**, XL280α x *sxi2***a**Δ, and
323 *sxi1*αΔ x *sxi2***a**Δ, respectively (TableS1). In contrast to the solo-cultures undergoing unisexual reproduction,
324 where DEGs were primarily upregulated in *sxi1*αΔ and *sxi2***a**Δ relative to wildtype, DEGs had both increased
325 and decreased expression relative to the XL280α x XL280**a** co-culture cross (Fig 5D-5F). GO term
326 enrichment analysis revealed that DEGs from the unilateral cross *sxi1*αΔ x XL280**a** were predominantly
327 associated with carbohydrate transport and metabolism, including monosaccharide, hexose, and glucose
328 transmembrane transport, as well as carbohydrate catabolic processes (S3B Fig). The unilateral cross
329 XL280α x *sxi2***a**Δ showed enrichment for broader carbohydrate metabolic and catabolic processes (S3B
330 Fig). In the bilateral mutant cross *sxi1*αΔ x *sxi2***a**Δ, enriched terms were similar to those in the *sxi1*αΔ
331 unilateral cross, with strong representation of carbohydrate transport, catabolism, and glucose-related
332 processes (S3B Fig). These results suggest that deletion of *SXI1*α has a more pronounced impact on
333 carbohydrate-related pathways during mating compared to deletion of *SXI2***a**. There were 8 DEGs in
334 common between solo *sxi1*αΔ and the *sxi1*αΔ x XL280**a** cross and 5 DEGs in common between solo *sxi2***a**Δ
335 and the XL280α x *sxi2***a**Δ cross (Fig 5G and 5H). These genes are largely uncharacterized, with functions
336 that remain unknown, except for *DHA1* (CND04870) [47], a secreted protein whose expression is regulated
337 by copper availability and which was identified as a DEG in both modes of sexual reproduction in the *sxi2***a**Δ
338 mutant. Comparison of the predicted protein sequences of these shared genes with *S. cerevisiae* proteins
339 shows potential orthologs with roles in metabolic processes (TableS2).

340 Given the enrichment for metabolic processes in the transcriptomic data, we used Biolog YT
341 phenotypic plates to assess whether these changes translated into altered substrate utilization [48,49]. The
342 Biolog YT panel is specifically designed for yeast metabolic phenotyping and contains 94 wells, each

343 preloaded with a different carbon source, enabling comprehensive assessment of both respiratory and
344 growth-based metabolic activity over time. PCA of metabolic activity at 72, 96, and 120 h showed partial
345 separation between *sxi1*αΔ and XL280α (PC1 = 24.4% variance) (S4A Fig), with PERMANOVA confirming
346 a significant difference ($R^2 = 0.123$, $p = 0.026$). *sxi2***a**Δ and XL280**a** showed greater overlap (PC1 = 43%)
347 (S4B Fig), with no significant difference ($R^2 = 0.057$, $p = 0.389$). To pinpoint the substrates contributing to
348 these differences, pairwise t-tests were performed for each carbon source at each time point. In the *sxi1*αΔ
349 mutant, significant differences ($p < 0.05$) compared to XL280α were observed for utilization of D-gluconic
350 acid, D-sorbitol, L-malic acid, N-acetyl-L-glutamic acid plus D-xylose, and palatinose at one or more tested
351 time points (S5 Fig). In the *sxi2***a**Δ mutant, utilization of β-methyl-D-glucoside, gentibiose, quinic acid plus
352 D-xylose, D-galactose, D-raffinose, D-sorbitol, and dextrin differed significantly from XL280**a** in at least one
353 of the tested time points (S6 Fig). These phenotypic differences in carbon source utilization are consistent
354 with the RNA-seq GO term enrichment results, which indicated that the Sxi1α and Sxi2**a** mutations affect
355 genes involved in carbohydrate transport and metabolism.

356 The identification of shared DEGs between unisexual and α-**a** sexual crosses indicates that Sxi1α,
357 and potentially Sxi2**a**, could have distinct transcriptional effects from their heterodimer interacting partner.
358 These observations, coupled with the computational prediction that Sxi1α and Sxi2**a** may be capable of
359 forming homodimers, led us to question the extent of Sxi1α- and Sxi2**a**-dependent transcriptional effects
360 occurring independently of the presence of a functional heterodimer interacting partner during α x **a** crosses.
361 To differentiate between transcriptional events dependent on the Sxi1α-Sxi2**a** heterodimer as opposed to
362 only Sxi1α or only Sxi2**a**, we examined the direction of differential expression in DEGs identified in one or
363 more crosses (Fig 5I). Compared to the XL280α x XL280**a** cross, candidate heterodimer-regulated genes
364 should undergo either a positive (heterodimer-repressed) or negative (heterodimer-activated) change in
365 expression in crosses lacking *SXI1*α*, SXI2***a**, or both (Fig 5I, top panel). By these criteria, we identified 57
366 and 65 potential heterodimer-repressed and -activated genes, respectively (Fig 5I, top panel). Consistent
367 with previous reports [26,29], *CLP1* (CNB01190) was among the set of heterodimer-activated genes. We
368 next reasoned that any genes whose expression depends only on Sxi1α would have either increased
369 (Sxi1α-repressed) or decreased (Sxi1α-activated) expression relative to wildtype in the *sxi1*αΔ x XL280**a**
370 cross, but no expression change in the XL280α x *sxi2***a**Δ cross because XL280α has a functional copy of

371 Sxi1α (Fig 5I, middle panel). Strikingly, we identified a larger gene set that fit these criteria than potential
372 heterodimer-regulated genes, with 78 and 109 Sxi1α-activated and -repressed DEGs, respectively (Fig 5I,
373 middle panel). Lastly, we applied similar reasoning to identify DEGs whose expression depends only on a
374 functional copy of *SXI2***a** (Fig 5I, bottom panel). From this comparison, we identified 14 and 27 potential
375 Sxi2**a**-activated and -repressed genes, respectively (Fig 5I, bottom panel). Surprisingly, *CPR2* (CNB04250)
376 [27], a gene thought to be activated by the Sxi1α-Sxi2**a** heterodimer, was present in the set of 27 genes
377 with potential Sxi2**a**-dependent activation.
378
379 ***SXI1*α and *SXI2*a have distinct regulatory effects on the α and a *MAT* loci**
380 We observed an enrichment of *MAT*α and *MAT***a** genes in the Sxi1α- and Sxi2**a**-only dependent
381 sets of DEGs compared to the heterodimer set, where only 2 genes (*MF***a***1* and *MF***a***2*) were predicted to
382 be heterodimer repressed (Fig 5I, top panel). Plotting expression change in all crosses for the *MAT*α and
383 *MAT***a** loci revealed an even more surprising pattern, where a majority of genes in each locus appear to be
384 controlled by Sxi1α and Sxi2**a** in opposing directions. *MAT*α genes tend to have increased expression in
385 the absence of Sxi1α and decreased expression in the absence of Sxi2**a**, suggesting a negative regulatory
386 role for Sxi1α and a positive regulatory role for Sxi2**a** (Fig. 5J). Conversely, *MAT***a** genes generally have
387 positive expression changes in the absence of Sxi2**a** and negative expression changes in the absence of
388 Sxi1α (Fig. 5K). In the case of *MAT***a** genes, expression differences in the *sxi1*αΔ x *sxi2***a**Δ more closely
389 mirror the XL280α x *sxi2***a**Δ cross than the *sxi1*αΔ x XL280**a** cross. Therefore, while *sxi2***a**Δ may result in a
390 smaller set of uniquely differentially expressed genes, Sxi2**a** may have an important role in driving *MAT***a**
391 gene expression change in opposition to Sxi1α. Taken together, these results support distinct roles for
392 *SXI1*α and *SXI2***a** in both mating-type-specific and more general gene regulation.

Discussion

The AlphaFold3-predicted heterodimer structure of Sxi1α and Sxi2**a** closely resembles the yeast **a**1-α2 complex [40] and the predicted *U. maydis* bW-bE heterodimer, consistent with prior studies [2,22]. This apparent conservation across diverse yeast species supports an evolutionarily important role of the Sxi1α-Sxi2**a** complex in α x **a** mating. Lower-confidence predictions indicate that Sxi1α and Sxi2**a** may also form homodimers, similar to α2 in *S. cerevisiae*, raising the possibility of independent, non-heterodimer functions. Interestingly, homodimerization of HD2 has been reported in the homothallic fungus *Cystofilobasidium capitatum*, where HD2 homodimers can substitute for the canonical HD1-HD2 heterodimer and thereby provide an alternative mechanism for regulating sexual reproduction [50]. Likewise, in the basidiomycetous yeast *Phaffia rhodozyma*, the homeodomain proteins HD1 and HD2 display only a weak heterodimer interaction, while experimental assays revealed potential homodimer formation [51]. In contrast, in *Ustilago maydis* the bE and bW homeodomain transcription factors strictly function through non-self heterodimerization, and no evidence for functional homodimerization has been found [52]. These examples suggest that HD homodimerization, although rare, may provide lineage-specific solutions for regulating sexual development. Together with our transcriptomic findings, this led us to hypothesize that these transcription factors can act both together and separately, regulating mating before and after cell-cell fusion in unisexual and α x **a** reproduction.

Our transcriptomic results provide further evidence for this model, as we observed Sxi2**a**-independent transcriptional regulation by Sxi1α and Sxi1α-independent regulation by Sxi2**a** in both unisexual and α-**a** sexual matings. In addition to regulating largely distinct gene sets, Sxi1α and Sxi2**a** exert contrasting effects on the two mating-type loci. We observed an enrichment of *MAT*α and *MAT***a** genes in the Sxi1α-only and Sxi2**a**-only dependent DEG sets in α-**a** crosses, whereas the heterodimer-dependent set contained only two repressed genes (*MF***a***1* and *MF***a***2*). Strikingly, most *MAT*α genes showed increased expression in the absence of *Sxi1*α but decreased expression in the absence of *Sxi2***a**, suggesting that Sxi1α functions primarily as a negative regulator and Sxi2**a** as a positive regulator at this locus. The pattern was reversed for *MAT***a** genes, with *Sxi1*α acting positively and *Sxi2***a** negatively. These results indicate that, beyond their shared role as a heterodimer, Sxi1α and Sxi2**a** also engage in mating-type-specific regulatory programs that act in opposition to each other, potentially fine-tuning the expression of *MAT*-linked

421 genes during α x **a** sexual reproduction. Deletion of Sxi1α caused an increase in α-α cell fusion, consistent
422 with a functional role beyond that of Sxi1α-Sxi2**a** heterodimer. These results support the possibility that
423 Sxi1α may form homodimers with distinct structure and function independent of Sxi2**a**. In α x **a** reproduction,
424 both Sxi1α and Sxi2**a** are essential for normal hyphal development and sporulation in multiple genetic
425 backgrounds [2,22]. In contrast, in the XL280 background, deletion of either gene did not impair unisexual
426 colony morphology or sporulation. These results, coupled with the observation of *SXI1*α - and *SXI2***a**-
427 dependent transcriptional activity during unisexual and α-**a** sexual reproduction, suggest that these
428 transcription factors are active but may play distinct roles in α x α and **a** x **a** versus α x **a** reproduction, and
429 that unisexual reproduction is likely regulated in a manner that is at least partially distinct from α x **a** sexual
430 reproduction. This is also consistent with recent reports that Sxi2**a** is dispensable for unisexual reproduction
431 in *C. neoformans* [31].

432 Functional differences between the two HD proteins were most evident in unisexual fusion assays.
433 Sxi1α inhibited fusion in both unilateral and bilateral mutant crosses, whereas Sxi2**a** inhibition was observed
434 only in unilateral crosses. This may indicate that Sxi2**a** plays a less-prominent or context-dependent role
435 in **a** x **a** cell fusion, possibly masked in bilateral crosses by redundancy with other transcription factors.
436 Testing this possibility will require identifying Sxi2**a**'s non-Sxi1α partners and determining their contributions
437 to fusion regulation.

438 Our transcriptomic analysis identified distinct subsets of Sxi1α- and Sxi2**a**-regulated genes in both
439 unilateral and bilateral crosses. A majority of these genes remain uncharacterized, inviting future functional
440 investigation into their potential involvement in cell-cell fusion ang sexual reproduction. Notably, GO term
441 enrichment highlighted metabolism-related processes, and Biolog YT plate profiling revealed subtle but
442 reproducible shifts in carbon source utilization between wildtype and mutants. Together, these findings
443 suggest that Sxi1α and Sxi2**a** influence metabolic pathways, which may, in turn, modulate mating efficiency
444 under nutrient-variable conditions, thereby linking metabolic state to the mating regulatory network. In
445 addition, *PRM1* (CNF01070) [53], a positive regulator of cell fusion, was activated in the absence of Sxi1α
446 and Sxi2**a** during co-culture condition, suggesting that these HD proteins may modulate fusion efficiency
447 by regulating downstream factors such as *PRM1*. Whether this regulation is direct or operates through
448 other transcriptional pathways is not yet clear.

449 By analyzing 341 *MAT*α clinical and environmental isolates out of the total 387 isolates in the *C.*
450 *neoformans* Strain Diversity Collection [33] through a similar pipeline as reported in our previous work [54],
451 we found there were only two closely related environmental isolates (Muc504-1 and Muc489-1) that
452 harbored an identical high-impact nonsense mutation in the *SXI1*α gene, resulting in truncation of the C-
453 terminal 23 amino acids. The widespread conservation of this gene suggests that it is under positive
454 selection and likely has important functions in a variety of ecological contexts. Unisexual reproduction,
455 which allows cells to produce stress-resistant spores under harsh environmental conditions in the absence
456 of an opposite mating type partner, provides one hypothetical avenue by which sex-specific genes like
457 *SXI1*α could continue to be selected for in a predominantly *MAT*α population. While the inhibitory role of
458 Sxi1α on unisexual α-α fusion could, in principle, be expected to limit the expansion of *MAT*α lineages and
459 favor *MAT***a** cells, this prediction appears inconsistent with the observed predominance of *MAT*α in natural
460 populations. This paradox suggests that additional mechanisms beyond Sxi1α regulation must contribute
461 to shaping the observed mating-type distribution. Further studies are needed to clarify the downstream
462 regulators involved in the novel repressive role of Sxi1α in unisexual reproduction and other potential
463 mating-independent functions. These lines of investigation have the potential to elucidate fitness-
464 enhancing strategies employed by this organism to undergo unisexual meiosis and produce infectious
465 spores. Over evolutionary time, it is conceivable that selection for alternative reproductive strategies such
466 as unisexual reproduction could have contributed to the widespread dominance of *MAT*α strains.

467 In *S. cerevisiae*, the α2 transcription factor functions both as a homodimer and heterodimer with
468 **a**1, playing key roles in mating-type regulation [6–9]. The transcriptional regulation of **a**-specific and
469 haploid-specific genes involves interactions with the transcription factor Mcm1 [6,55]. Given this precedent,
470 a similar dual functionality with/without mating partner may exist for the sex-specific HD transcription factor
471 Sxi1α in *Cryptococcus*, and non-Sxi2**a** interacting partners may exist. Interestingly, orthologs of *S.*
472 *cerevisiae* Mcm1 are also present in *C. neoformans* and *C. deneoformans*, where they have been reported
473 to function in α x **a** sexual reproduction [56]. Our AlphaFold structural prediction and alignment suggest a
474 conserved structural organization conserved between the *S. cerevisiae* α2-Mcm1 heterotetramer [57] and
475 the *C. deneoformans* Sxi1α-Mcm1 heterotetramer (S7 Fig). Further studies will be required to dissect the
476 molecular basis of the Sxi1α-Mcm1 interaction and its role within the broader regulatory network in

477 *Cryptococcus*. Our results suggest that Sxi1α might act as both a positive (e.g., in α x **a** mating
478 development) and a negative regulator (e.g., in α x α cell fusion) [23]. This phenomenon is reminiscent of
479 the mitogen-activated protein kinase Kss1 in *S. cerevisiae*, which regulates pseudohyphal differentiation
480 through complex signaling mechanisms and functions as a multifunctional regulator in fungal development
481 with counter-balanced positive and negative roles [58]. Efforts to identify potential Sxi1α - and Sxi2**a** -
482 specific transcription factor binding sites in the promoter regions of differentially expressed genes were not
483 unsuccessful. We hypothesize that our inability to identify distinctive binding motifs in these gene sets is
484 due to the activation of regulatory cascades as a result of changes in Sxi1α and Sxi2**a** activity, meaning
485 that many promoters of DEGs are not bound by the homeodomain proteins themselves. Future efforts to
486 elucidate direct targets of the heterodimer and putative homodimers will involve direct experimental
487 verification of the specific regions bound in the presence and absence of each transcription factor.

488 Taken together, while the HD proteins Sxi1α and Sxi2**a** are dispensable for colony morphology,
489 sporulation, and cell viability during unisexual reproduction, Sxi1α plays a key inhibitory role in α x α cell
490 fusion, while the contribution of Sxi2**a** to this process appears to be more limited. RNA-seq analysis further
491 revealed that the heterodimer partners also have distinct and independent regulatory programs, supporting
492 functional roles beyond their shared activity as a complex. These findings suggest that Sxi1α may have
493 novel functions during *Cryptococcus* mating that are yet to be characterized, echoing those in other well
494 studied fungal species and highlighting the regulatory complexity of sexual reproduction in this important
495 human fungal pathogen. Our findings further suggest that homeodomain factors may play broader roles in
496 both ascomycetes and basidiomycetes given the apparent conserved homeodomain function of **a**1-α2 in *S.*
497 *cerevisiae* and Sxi1α-Sxi2**a** in C. *deneoformans*.

498 **Materials and methods**

499 **Fungal strains and growth conditions**

500 *C. deneoformans* and *C. neoformans* strains for this study are listed in Table S3. The strains were
501 stored in 15% glycerol at -80°C for long-term storage. Fresh strains were streaked from glycerol stocks
502 and maintained on solid YPD medium (1% yeast extract, 2% Bacto Peptone, 2% dextrose) at 30°C.

503 Spot dilution assays were performed with overnight cultures of the tested strains grown in liquid
504 YPD at 30°C. Strains were diluted to an OD_{600} of 0.5 in sterile water. These cultures were further serially
505 diluted 5-fold and spotted (3 μL for each dilution) onto YPD plates. The plates were incubated at 30°C and
506 37°C (testing thermotolerance) for 2 days before imaging.

507

508 **Protein structural predictions**

509 Protein structure predictions were made with AlphaFold3 [59] on the AlphaFold server
510 (https://alphafoldserver.com/). The predicted models and error plots were further processed with Chimera
511 X (v 1.9) [60] for predicted local distance difference test (pLDDT) value filtering, alignment, and visualization.

512

513 **Gene deletion and confirmation**

514 Approximately 1.0 kb 5' and 3' flanking regions of the *SXI1*α gene and 60 bp 5' and 3' flanking
515 regions of the *SXI2***a** gene were constructed with primers listed in Table S4 to target their respective genes
516 for homologous recombination [61]. Overlap PCR with a selectable marker was used to construct the DNA
517 donor with 1.0 kb homology, while 60 bp microhomology was included in the primers for donor amplification.
518 *C. neoformans* codon optimized Cas9, gRNAs (a single gRNA targeting *SXI1*α and two gRNAs targeting
519 *SXI2***a**), and drug resistance cassettes (*NAT* from pAI3 or *NEO* from pJAF1) containing homologous flanking
520 sequences were introduced into XL280 wildtype strains via the previously reported Transient CRISPR-Cas9
521 Coupled with Electroporation (TRACE) system [38,39]. Transformants were screened with PCR internal to
522 the ORF, and 5′ and 3′ junction PCR to the drug resistance marker integration sites to confirm integration
523 at the genomic locus. Illumina whole-genome sequencing was performed on positive transformants with
524 Novaseq X Plus platform (2x150 bp). The sequencing reads were mapped to a modified version of the
525 XL280α genome [45] with the Burrows-Wheeler Alignment tool (BWA) (v 0.7.17) [62] to further confirm the

526 deletion mutant strains. The modification included adding the *MAT***a** locus sequence of JEC20 (GenBank:
527 AF542530.2) as an additional contig.
528
529 **Capsule formation and melanin production assays**
530 Tested strains, with an initial OD_{600} of 0.1 in 4 mL liquid RPMI medium (RPMI 1640 with 2%
531 dextrose), were incubated on a roller drum at 70 rpm and 30°C for 3 days. After washing and resuspension
532 in water, the cells were negatively stained with an equal volume of India ink to visualize the capsules.
533 To assess melanin production, overnight saturated cultures of test strains were spotted (10 μL)
534 onto Niger seed agar plates (7% Niger seed, 0.1% dextrose). The Niger seed plates were incubated at
535 30°C and 37°C for 8 days before photographing.
536
537 **Competition assays**
538 Overnight cultures of tested strains grown in liquid YPD at 30°C were diluted to OD_{600} of 0.2 and
539 equally mixed in a 1:1 ratio in 5 mL of liquid YPD for co-culture. *sxi1*αΔ::*NAT* mutants (resistant to NAT)
540 and *sxi2***a**Δ::*NEO* mutants (resistant to NEO) were mixed with XL280α and XL280**a**, respectively. The
541 mixture was plated on YPD plates, YPD + nourseothricin (NAT), and YPD + neomycin (NEO) to confirm
542 starting ratio. After 24 and 48 hours of co-culture, an aliquot of the mixture was sampled, and plating was
543 repeated with OD_{600} diluted to 0.1 to track changes in relative abundance of mutants. Four independent
544 replicates were performed for each competition.
545 For the competition assay performed on MS medium, overnight cultures were similarly diluted to
546 OD_{600} of 1. *sxi1*αΔ::*NAT* or *sxi2***a**Δ::*NEO* mutants and the corresponding XL280 wildtype strain were equally
547 mixed in a 1:1 ratio and spotted on MS medium. Spores were dissected 10 to 14 days post spotting. Yeast
548 cells from internal regions were also collected. Spores or yeast cells were further transferred to YPD+NAT,
549 YPD+NEO and YPD to determine the ratio of mutants in the population. Five independent spots were
550 investigated for each competition.
551
552
553

554 **Mating and cell-cell fusion assay**

555 Mating plates were set up as described previously [63]. α x α and **a** x **a** unisexual reproduction
556 assays were performed on Murashige and Skoog (MS, Sigma, USA) plates for 1 to 2 weeks before imaging
557 and dissection. Basidiospores generated during unisexual reproduction were randomly dissected and
558 plated on YPD plates for 2 to 3 days to determine spore viability and germination rates.

559 Cell-cell fusion frequency during α x α unisexual outcrossing in XL280α *NAT* (XL561 and XL562)
560 and XL280α *NEO* (XL563 and XL564) was compared to bilateral mutant crosses of *sxi1*αΔ::*NAT* and *sxi1*αΔ:
561 *NEO* or unilateral crosses of *sxi1*αΔ::*NAT* and XL280α *NEO*. Similarly, **a** x **a** unisexual outcrossing in
562 XL280**a** *NAT* (CF1816) and XL280**a** *NEO* (JHG223) was compared to bilateral mutant crosses of
563 *sxi2***a**Δ::*NAT* and *sxi2***a**Δ::*NEO* or unilateral crosses of *sxi2***a**Δ::*NAT* and XL280**a** *NEO* or *sxi2***a**Δ::*NEO* and
564 XL280**a** *NAT*.

565 Cells were diluted in sterile water to an OD_{600} of 1. Two *MAT*α strains (α x α outcrossing) or *MAT***a**
566 strains (**a** x **a** outcrossing) containing either *NAT* or *NEO* resistance cassettes were mixed equally with
567 JEC20 (*MAT***a**) or JEC21 (*MAT*α) for Ménage à trois matings on V8 agar (pH = 7.0) and incubated for 72
568 hours in the dark at room temperature. The cells were then collected and plated on YPD + NAT (100 μg/mL)
569 + NEO (200 μg/mL) and YPD alone to determine the ratio of colonies with dual resistance four to five days
570 post-plating (i.e., fusion product) out of the total cells. Genotypes at mating type locus of the fusion products
571 was validated via *STE20***a** or *STE20*α genotyping PCR.

572

573 **Flow cytometry analysis**

574 Ploidy of the fusion products from α x α or **a** x **a** cell fusion was determined by fluorescence-
575 activated cell sorting (FACS) analysis as previously described [64]. Cells were grown overnight on solid
576 YPD medium at 30 °C, harvested, and washed with 1 mL PBS. The cells were fixed in 70% ethanol at 4 °C
577 overnight, pelleted and washed with 1 x NS buffer (10 mM Tris-HCl pH=7.5, 0.25 M sucrose, 1 mM EDTA,
578 1 mM $MgCl_2$, 0.13 mM $CaCl_2$, 0.1 mM $ZnCl_2$, 0.5 mM phenylmethylsulfonyl fluoride, 7 mM β-
579 mercaptoethanol). Samples were treated with RNase A (1.05 mg/mL) and stained with propidium iodide
580 (PI, 30 μg/mL) in a total volume of 200 μL 1x NS solution. Stained cells were diluted in 1x Tris-PI buffer
581 (0.964 M Tris-HCl pH=7.5, 35 μg/mL PI) prior to analysis. FACS was performed at Duke Cancer Institute

582 Flow Cytometry Core Facility with approximately 10,000 cells analyzed per sample. Flow cytometry data
583 were visualized using FlowJo (v.10.10.0).
584
585 **Light and scanning electron microscopy (SEM)**
586 Mating structures from MS plates were imaged with an AxioSkop 2 fluorescence microscope to
587 visualize hyphae, basidia and basidiospores under brightfield. SEM samples were prepared following a
588 previously described protocol [44] with minor modifications. Briefly, a ~2 cm x 2 cm agar plug containing
589 patch of mated cells from MS plates was fixed in PBS containing 4% formaldehyde and 2% glutaraldehyde
590 at 4°C for 2 hours. The fixed samples were then gradually dehydrated in a graded ethanol series (30%,
591 50%, 70%, 95%), with each step performed at 4°C for 15 min. This was followed by three washes in 100%
592 ethanol, each at 4°C for 15 min. The samples were further dehydrated with a Ladd CPD3 Critical Point
593 Dryer and subsequently coated with a thin layer of gold with a Denton Desk V Sputter Coater (Denton
594 Vacuum, USA). Hyphae, basidia and basidiospores were observed with a scanning electron microscope
595 equipped with an EDS detector (Apreo S, ThermoFisher, USA).
596
597 **RNA preparation and sequencing**
598 For both unisexual and α x **a** sexual crosses, strains were collected from 2-3-day-old cultures
599 grown on solid YPD medium and diluted to an OD_{600} of 1. For unisexual crosses, 10 μL of the diluted culture
600 (OD_{600}=1) was spotted onto V8 agar plates (pH 7.0), with 10 spots per plate and three technical replicate
601 plates per biological replicate. For α x **a** crosses, equal volumes of *MAT*α and *MAT***a** cell suspensions
602 (each at OD_{600}=1) were mixed prior to spotting under the same conditions. Three biological replicates were
603 performed for each strain or mating pair. Plates were incubated at room temperature for 72 hours in the
604 dark, after which cells were washed off and collected. Harvested samples were lyophilized and processed
605 for RNA extraction using the RNeasy Mini Kit (Qiagen), following the manufacturer's instructions.
606 RNA was sequenced by the Duke University Sequencing and Genomic Technologies Core Facility.
607 Poly-A enriched libraries were prepared from samples with RIN ≥ 7 using the Kapa mRNA-seq HyperPrep
608 kit (Kapa Bioscience). Pooled libraries were sequenced on an Illumina Novaseq X Plus instrument in 150
609 bp paired-end reads.

610 **RNA-sequencing data analysis**

611 Illumina universal adaptors were trimmed from paired reads with CutAdapt (v4.9) [65]. Trimmed
612 reads were aligned to the XL280α + *MAT***a** concatenated reference assembly. Modified assemblies with
613 *MAT*α (Chr4 coordinates 1522691-1656182) and *MAT***a** (MATa coordinates 0-148067) masked were
614 generated by using the bedtools (v2.31.1) maskfasta function on the concatenated assembly [66]. XL280α
615 background unisexual crosses were mapped to the *MAT***a**-masked assembly, XL280**a** background
616 unisexual crosses to the *MAT*α-masked assembly, and α-**a** sexual crosses to the full, unmasked assembly
617 with HISAT2 (v2.2.1) [67]. Counts per gene were quantified with featureCounts (v2.0.6) [68] with a gff
618 annotation file generated by Liftoff (v1.6.3) [69] of annotated features from JEC20 and JEC21 [70].

619 Exploratory data analysis and differential expression analysis were performed with DESeq2
620 (v1.44.0) [71]. Prior to analysis, transcript counts were normalized by transcripts per million (TPM) within
621 each replicate and genes with at least 1 TPM in 1 sample were retained. Clustering and principal
622 component analyses were performed using vst normalized values for the top 500 most variable genes
623 generated by DESeq2. Differential expression analysis was carried out in DESeq2 with alpha = 0.05 and
624 a $\log_2$FC cutoff of +/- 1 was applied to identify DEGs from the resulting expression data. The R packages
625 EnhancedVolcano (v1.22.0) (https://github.com/kevinblighe/EnhancedVolcano) and pheatmap (v1.0.13)
626 (https://github.com/raivokolde/pheatmap) were used for data visualization. DEG sets were analyzed with
627 the FungiDB (https://fungidb.org/fungidb/app) GO Enrichment tool using the JEC21 genome as background.
628 Significance was assessed using Fisher's exact test with Benjamini-Hochberg correction, retaining terms
629 with FDR < 0.05. Enriched terms were visualized in RStudio as dot plots ranked by $\log_2$(fold enrichment)
630 or FDR, colored by $-\log_{10}$(FDR), and annotated with gene counts.

631

632 **Biolog phenotypic assays**

633 Overnight cultures grown on solid YM agar (5 g peptone, 3 g yeast extract, 3 g malt extract, 10 g
634 dextrose, 20g agar, pH=6.2) were collected and diluted in sterile water to an OD_{600} of 0.2. A volume of 100
635 µL of the diluted samples was inoculated into each well of the Biolog Yeast Identification Test Panel (YT
636 Microplate) and cultured at 28 °C in the dark. Three biological replicates were performed for each strain.

637 Cell growth was monitored daily with SpectraMax iD3 plate reader at OD_{590} (oxidation test) and
638 OD_{600} (Assimilation test). Growth on each substrate was normalized using the formula (Abs_sample -
639 Abs_water)/(Abs_glucose-Abs_water). Principal component analysis (PCA) was performed using scaled
640 data from Biolog YT plate assays. Differences in global metabolic profiles between genotypes were
641 assessed using PERMANOVA (adonis2 function, vegan R package), with 999 permutations and Euclidean
642 distance as the dissimilarity metric.
643
644 **Statistical analysis**
645 Spore germination and unisexual competitiveness were analyzed with paired or unpaired student
646 t-tests in Rstudio (version 2024.04.1) with the “t.test” function with argument “paired = TRUE” for paired
647 tests or “paired = FALSE” for unpaired tests.
648 Fusion efficiency data were analyzed in RStudio (version 2024.04.1). Welch’s t-tests were
649 performed using the t.test function with the argument “var.equal = FALSE” to compare fusion rates between
650 selected sample groups. Mean values and standard deviations were plotted using ggplot2, with individual
651 data points overlaid.

652 **Data availability**

653 Raw WGS sequencing and RNA-seq reads have been deposited in Bioproject: PRJNA1219566.
654 All programming scripts associated with this project are available at:
655 https://github.com/annalehmann/XL280_Sxi_transcriptome.

656

657 **Acknowledgments**

658 We thank Anna Floyd Averette for constant support, Connor Larmore for critical reading, Dr. Marco
659 Dias Coelho for constructive criticism on the manuscript and suggestions on data presentation, Moayad
660 Shehadeh and Dr. Zhuyun Bian for technical support, and all of the members of the Heitman Lab for
661 constructive suggestions. We also thank Dr. Xiaorong Lin (University of Georgia) for sharing the XL280
662 congenic strains, Dr. Ruiyun Zeng (North Carolina State University) for assistance in data visualization, Dr.
663 Paul Magwene and Claudia Zirión Martinez (Department of Biology, Duke) for sharing unpublished pipeline
664 for variant detection from Strain Diversity Collection, Dr. Bin Li (Duke Cancer Institute Flow Cytometry Core
665 Facility), Julian Liber (Department of Biology, Duke), and Dr. Devi Swain Lenz (Duke's Sequencing and
666 Genomic Technologies Core Facility) for advice and expertise.

667

668 **Funding**

669 This study was supported by NIH/NIAID R01 grants AI039115-28, AI050113-20, and AI133654-07.
670 J. Heitman is co-director and fellow of the Canadian Institute for Advanced Research (CIFAR) program
671 Fungal Kingdom: Threats & Opportunities.

672

673 **Conflict of Interest**

674 The authors declare no conflicts of interest.

675 **References**

676 1. Coelho MA, David-Palma M, Marincowitz S, Aylward J, Pham NQ, Yurkov AM, et al. Tracing the
677 evolution and genomic dynamics of mating-type loci in *Cryptococcus* pathogens and closely related
678 species. bioRxiv; 2025. doi:10.1101/2025.02.12.637874
679 2. Hull CM, Boily M-J, Heitman J. Sex-Specific homeodomain proteins Sxi1α and Sxi2**a** coordinately
680 regulate sexual development in *Cryptococcus neoformans*. Eukaryot Cell. 2005;4: 526–535.
681 doi:10.1128/EC.4.3.526-535.2005
682 3. Yadav V, Sun S, Heitman J. On the evolution of variation in sexual reproduction through the prism of
683 eukaryotic microbes. Proc Natl Acad Sci USA. 2023;120: e2219120120.
684 doi:10.1073/pnas.2219120120
685 4. Goutte C, Johnson AD. a1 protein alters the dna binding specificity of α2 repressor. Cell. 1988;52:
686 875–882. doi:10.1016/0092-8674(88)90429-1
687 5. Li T, Stark MR, Johnson AD, Wolberger C. Crystal structure of the MATa1/MATα2 homeodomain
688 heterodimer bound to DNA. Science. 1995;270: 262–269. doi:10.1126/science.270.5234.262
689 6. Keleher CA, Goutte C, Johnson AD. The yeast cell-type-specific repressor α2 acts cooperatively
690 with a non-cell-type-specific protein. Cell. 1988;53: 927–936. doi:10.1016/S0092-8674(88)90449-7
691 7. Herskowitz I. A regulatory hierarchy for cell specialization in yeast. Nature. 1989;342: 749–757.
692 doi:10.1038/342749a0
693 8. Goutte C, Johnson AD. Yeast a1 and α2 homeodomain proteins form a DNA-binding activity with
694 properties distinct from those of either protein. Journal of Molecular Biology. 1993;233: 359–371.
695 doi:10.1006/jmbi.1993.1517
696 9. Dranginis AM. Binding of yeast a1 and α2 as a heterodimer to the operator DNA of a haploid-
697 specific gene. Nature. 1990;347: 682–685. doi:10.1038/347682a0
698 10. Gillissen B, Bergemann J, Sandmann C, Schroeer B, Bölker M, Kahmann R. A two-component
699 regulatory system for self/non-self recognition in *Ustilago maydis*. Cell. 1992;68: 647–657.
700 doi:10.1016/0092-8674(92)90141-X
701 11. Kämper J, Reichmann M, Romeis T, Bölker M, Kahmann R. Multiallelic recognition: Nonself-
702 dependent dimerization of the bE and bW homeodomain proteins in *Ustilago maydis*. Cell. 1995;81:
703 73–83. doi:10.1016/0092-8674(95)90372-0
704 12. Wahl R, Zahiri A, Kämper J. The *Ustilago maydis b* mating type locus controls hyphal proliferation
705 and expression of secreted virulence factors *in planta*. Molecular Microbiology. 2010;75: 208–220.
706 doi:10.1111/j.1365-2958.2009.06984.x
707 13. Vollmeister E, Schipper K, Baumann S, Haag C, Pohlmann T, Stock J, et al. Fungal development of
708 the plant pathogen *Ustilago maydis*. FEMS Microbiol Rev. 2012;36: 59–77. doi:10.1111/j.1574-
709 6976.2011.00296.x
710 14. Kües U, Göttgens B, Stratmann R, Richardson WV, O'Shea SF, Casselton LA. A chimeric
711 homeodomain protein causes self-compatibility and constitutive sexual development in the
712 mushroom *Coprinus cinereus*. EMBO J. 1994;13: 4054–4059. doi:10.1002/j.1460-
713 2075.1994.tb06722.x
714 15. Francisco EC, de Jong AW, Hagen F. Cryptococcosis and *Cryptococcus*. Mycopathologia.
715 2021;186: 729–731. doi:10.1007/s11046-021-00577-7
716 16. Brown GD, Ballou ER, Bates S, Bignell EM, Borman AM, Brand AC, et al. The pathobiology of
717 human fungal infections. Nat Rev Microbiol. 2024;22: 687–704. doi:10.1038/s41579-024-01062-w
718 17. Sun S, Coelho MA, David-Palma M, Priest SJ, Heitman J. The evolution of sexual reproduction and
719 the mating-type Locus: links to pathogenesis of *Cryptococcus* human pathogenic fungi. Annu Rev
720 Genet. 2019;53: 417–444. doi:10.1146/annurev-genet-120116-024755
721 18. Bian Z, Xu Z, Peer A, Choi Y, Priest SJ, Akritidou K, et al. Essential genes encoded by the mating-
722 type locus of the human fungal pathogen *Cryptococcus neoformans*. Genetics; 2024.
723 doi:10.1101/2024.12.02.626420
724 19. Sun S, Coelho MA, David-Palma M, Huang J, Bian Z, Heitman J. Fungal sexual reproduction and
725 mating-type loci. Current Biology. 2025;35: R496–R503. doi:10.1016/j.cub.2025.04.061
726 20. Kwon-Chung KJ, Bennett JE. Distribution of alpha and alpha mating types of *Cryptococcus*
727 *neoformans* among natural and clinical isolates. American Journal of Epidemiology. 1978;108: 337–
728 340. doi:10.1093/oxfordjournals.aje.a112628

21. Yan Z, Hull CM, Heitman J, Sun S, Xu J. *SXI1*α controls uniparental mitochondrial inheritance in *Cryptococcus neoformans*. Current Biology. 2004;14: R743–R744. doi:10.1016/j.cub.2004.09.008
22. Hull CM, Davidson RC, Heitman J. Cell identity and sexual development in *Cryptococcus neoformans* are controlled by the mating-type-specific homeodomain protein Sxi1α. Genes Dev. 2002;16: 3046–3060. doi:10.1101/gad.1041402
23. Hull CM, Cox GM, Heitman J. The α-specific cell identity factor Sxi1α is not required for virulence of *Cryptococcus neoformans*. Infect Immun. 2004;72: 3643–3645. doi:10.1128/IAI.72.6.3643-3645.2004
24. Sun S, Fu C, Ianiri G, Heitman J. The pheromone and pheromone receptor mating-type locus is involved in controlling uniparental mitochondrial inheritance in *Cryptococcus*. Genetics. 2020;214: 703–717. doi:10.1534/genetics.119.302824
25. Hsueh Y-P, Fraser JA, Heitman J. Transitions in sexuality: recapitulation of an ancestral tri- and tetrapolar mating system in *Cryptococcus neoformans*. Eukaryot Cell. 2008;7: 1847–1855. doi:10.1128/EC.00271-08
26. Ekena JL, Stanton BC, Schiebe-Owens JA, Hull CM. Sexual development in *Cryptococcus neoformans* requires *CLP1* , a target of the homeodomain transcription factors Sxi1α and Sxi2**a**. Eukaryot Cell. 2008;7: 49–57. doi:10.1128/EC.00377-07
27. Hsueh Y-P, Xue C, Heitman J. A constitutively active GPCR governs morphogenic transitions in *Cryptococcus neoformans*. EMBO J. 2009;28: 1220–1233. doi:10.1038/emboj.2009.68
28. Heimel K, Scherer M, Schuler D, Kämper J. The *Ustilago maydis* Clp1 protein orchestrates pheromone and *b* -dependent signaling pathways to coordinate the cell cycle and pathogenic development. The Plant Cell. 2010;22: 2908–2922. doi:10.1105/tpc.110.076265
29. Mead ME, Stanton BC, Kruzel EK, Hull CM. Targets of the Sex Inducer homeodomain proteins are required for fungal development and virulence in *Cryptococcus neoformans*. Mol Microbiol. 2015;95: 804–818. doi:10.1111/mmi.12898
30. Lin X, Hull CM, Heitman J. Sexual reproduction between partners of the same mating type in *Cryptococcus neoformans*. Nature. 2005;434: 1017–1021. doi:10.1038/nature03448
31. Sun S, Bian Z, Xu Z, Choi Y, Heitman J. Unisexual reproduction in the global human fungal pathogen *Cryptococcus neoformans*. bioRxiv; 2025. doi:10.1101/2025.06.02.657540
32. Sun S, Roth C, Floyd Averette A, Magwene PM, Heitman J. Epistatic genetic interactions govern morphogenesis during sexual reproduction and infection in a global human fungal pathogen. Proc Natl Acad Sci USA. 2022;119: e2122293119. doi:10.1073/pnas.2122293119
33. Desjardins CA, Giamberardino C, Sykes SM, Yu C-H, Tenor JL, Chen Y, et al. Population genomics and the evolution of virulence in the fungal pathogen *Cryptococcus neoformans*. Genome Res. 2017;27: 1207–1219. doi:10.1101/gr.218727.116
34. Hitchcock M, Veronica Thorn, Himeshi Samarasinghe, Sheng Sun, Joseph Heitman, Jianping Xu. Genomic evidence for a-α heterothallic and α-α unisexual mating and recombination in an environmental *Cryptococcus deneoformans* population. bioRxiv. 2025. doi:https://doi.org/10.1101/2025.08.20.671223
35. Sun S, Billmyre RB, Mieczkowski PA, Heitman J. Unisexual reproduction drives meiotic recombination and phenotypic and karyotypic plasticity in *Cryptococcus neoformans*. Butler G, editor. PLoS Genet. 2014;10: e1004849. doi:10.1371/journal.pgen.1004849
36. Roth C, Sun S, Billmyre RB, Heitman J, Magwene PM. A high-resolution map of meiotic recombination in *Cryptococcus deneoformans* demonstrates decreased recombination in unisexual reproduction. Genetics. 2018;209: 567–578. doi:10.1534/genetics.118.300996
37. Zhai B, Zhu P, Foyle D, Upadhyay S, Idnurm A, Lin X. Congenic strains of the filamentous form of *Cryptococcus neoformans* for studies of fungal morphogenesis and virulence. Infect Immun. 2013;81: 2626–2637. doi:10.1128/IAI.00259-13
38. Huang MY, Joshi MB, Boucher MJ, Lee S, Loza LC, Gaylord EA, et al. Short homology-directed repair using optimized Cas9 in the pathogen *Cryptococcus neoformans* enables rapid gene deletion and tagging. Genetics. 2022;220: iyab180. doi:10.1093/genetics/iyab180
39. Fan Y, Lin X. Multiple applications of a transient CRISPR-Cas9 coupled with electroporation (TRACE) system in the *Cryptococcus neoformans* species complex. Genetics. 2018;208: 1357–1372. doi:10.1534/genetics.117.300656
40. Li T. Crystal structure of the MATa1/MATalpha2 homeodomain heterodimer in complex with DNA containing an A-tract. Nucleic Acids Research. 1998;26: 5707–5718. doi:10.1093/nar/26.24.5707

41. Huang J, Rowe D, Subedi P, Zhang W, Suelter T, Valent B, et al. CRISPR-Cas12a induced DNA double-strand breaks are repaired by multiple pathways with different mutation profiles in *Magnaporthe oryzae*. Nat Commun. 2022;13: 7168. doi:10.1038/s41467-022-34736-1
42. Xue C, Tada Y, Dong X, Heitman J. The human fungal pathogen *Cryptococcus* can complete its sexual cycle during a pathogenic association with plants. Cell Host & Microbe. 2007;1: 263–273. doi:10.1016/j.chom.2007.05.005
43. Phadke SS, Feretzaki M, Heitman J. Unisexual reproduction enhances fungal competitiveness by promoting habitat exploration via hyphal growth and sporulation. Eukaryot Cell. 2013;12: 1155–1159. doi:10.1128/EC.00147-13
44. Peterson PP, Choi J-T, Fu C, Cowen LE, Sun S, Bahn Y-S, et al. The *Cryptococcus neoformans* STRIPAK complex controls genome stability, sexual development, and virulence. PLoS Pathog. 2024;20: e1012735. doi:10.1371/journal.ppat.1012735
45. Fu C, Davy A, Holmes S, Sun S, Yadav V, Gusa A, et al. Dynamic genome plasticity during unisexual reproduction in the human fungal pathogen *Cryptococcus deneoformans*. PLoS Genet. 2021;17: e1009935. doi:10.1371/journal.pgen.1009935
46. Rutherford JC, Lin X, Nielsen K, Heitman J. Amt2 permease is required to induce ammonium-responsive invasive growth and mating in *Cryptococcus neoformans*. Eukaryot Cell. 2008;7: 237–246. doi:10.1128/EC.00079-07
47. Gyawali R, Upadhyay S, Way J, Lin X. A family of secretory proteins Is associated with different morphotypes in *Cryptococcus neoformans*. Schottel JL, editor. Appl Environ Microbiol. 2017;83: e02967-16. doi:10.1128/AEM.02967-16
48. Coelho MA, David-Palma M, Kachalkin AV, Kolařík M, Turchetti B, Sampaio JP, et al. Genomic and phenotypic insights into the expanding phylogenetic landscape of the *Cryptococcus* genus. bioRxiv; 2025. doi:10.1101/2025.06.18.660340
49. Mackie AM, Hassan KA, Paulsen IT, Tetu SG. Biolog phenotype microarrays for phenotypic characterization of microbial cells. Methods Mol Biol. 2014;1096: 123–130. doi:10.1007/978-1-62703-712-9_10
50. Cabrita A, David-Palma M, Brito PH, Heitman J, Coelho MA, Gonçalves P. Multiple pathways to homothallism in closely related yeast lineages in the basidiomycota. mBio. 2021;12: e03130-20. doi:10.1128/mBio.03130-20
51. David-Palma M, Sampaio JP, Gonçalves P. Genetic dissection of sexual reproduction in a primary homothallic basidiomycete. PLoS Genet. 2016;12: e1006110. doi:10.1371/journal.pgen.1006110
52. Gillissen B, Bergemann J, Sandmann C, Schroeer B, Bölker M, Kahmann R. A two-component regulatory system for self/non-self recognition in Ustilago maydis. Cell. 1992;68: 647–657. doi:10.1016/0092-8674(92)90141-X
53. Fu C, Heitman J. PRM1 and KAR5 function in cell-cell fusion and karyogamy to drive distinct bisexual and unisexual cycles in the *Cryptococcus* pathogenic species complex. PLoS Genet. 2017;13: e1007113. doi:10.1371/journal.pgen.1007113
54. Huang J, Larmore CJ, Priest SJ, Xu Z, Dietrich FS, Yadav V, et al. Distinct evolutionary trajectories following loss of RNA interference in *Cryptococcus neoformans*. Proc Natl Acad Sci USA. 2024;121: e2416656121. doi:10.1073/pnas.2416656121
55. Elble R, Tye BK. Both activation and repression of a-mating-type-specific genes in yeast require transcription factor Mcm1. Proc Natl Acad Sci USA. 1991;88: 10966–10970. doi:10.1073/pnas.88.23.10966
56. Jung K-W, Yang D-H, Maeng S, Lee K-T, So Y-S, Hong J, et al. Systematic functional profiling of transcription factor networks in *Cryptococcus neoformans*. Nat Commun. 2015;6: 6757. doi:10.1038/ncomms7757
57. Tan S, Richmond TJ. Crystal structure of the yeast MATα2/MCM1/DNA ternary complex. Nature. 1998;391: 660–666. doi:10.1038/35563
58. Madhani HD, Styles CA, Fink GR. MAP kinases with distinct Inhibitory functions impart signaling specificity during yeast differentiation. Cell. 1997;91: 673–684. doi:10.1016/S0092-8674(00)80454-7
59. Abramson J, Adler J, Dunger J, Evans R, Green T, Pritzel A, et al. Accurate structure prediction of biomolecular interactions with AlphaFold 3. Nature. 2024;630: 493–500. doi:10.1038/s41586-024-07487-w
60. Meng EC, Goddard TD, Pettersen EF, Couch GS, Pearson ZJ, Morris JH, et al. UCSF ChimeraX: Tools for structure building and analysis. Protein Science. 2023;32: e4792. doi:10.1002/pro.4792

841 61. Huang J, Cook DE. The contribution of DNA repair pathways to genome editing and evolution in
842 filamentous pathogens. FEMS Microbiol Rev. 2022;46: fuac035. doi:10.1093/femsre/fuac035
843 62. Li H, Durbin R. Fast and accurate short read alignment with Burrows–Wheeler transform.
844 Bioinformatics. 2009;25: 1754–1760. doi:10.1093/bioinformatics/btp324
845 63. Sun S, Priest SJ, Heitman J. *Cryptococcus neoformans* mating and genetic Crosses. Current
846 Protocols in Microbiology. 2019;53: e75. doi:10.1002/cpmc.75
847 64. Tanaka R, Taguchi H, Takeo K, Miyaji M, Nishimura K. Determination of ploidy in *Cryptococcus*
848 *neoformans* by flow cytometry. J Med Vet Mycol. 1996;34: 299–301.
849 65. Kechin A, Boyarskikh U, Kel A, Filipenko M. cutPrimers: A new tool for accurate cutting of primers
850 from reads of targeted next generation sequencing. Journal of Computational Biology. 2017;24:
851 1138–1143. doi:10.1089/cmb.2017.0096
852 66. Quinlan AR, Hall IM. BEDTools: a flexible suite of utilities for comparing genomic features.
853 Bioinformatics. 2010;26: 841–842. doi:10.1093/bioinformatics/btq033
854 67. Kim D, Paggi JM, Park C, Bennett C, Salzberg SL. Graph-based genome alignment and genotyping
855 with HISAT2 and HISAT-genotype. Nat Biotechnol. 2019;37: 907–915. doi:10.1038/s41587-019-
856 0201-4
857 68. Liao Y, Smyth GK, Shi W. featureCounts: an efficient general purpose program for assigning
858 sequence reads to genomic features. Bioinformatics. 2014;30: 923–930.
859 doi:10.1093/bioinformatics/btt656
860 69. Shumate A, Salzberg SL. Liftoff: accurate mapping of gene annotations. Bioinformatics. 2021;37:
861 1639–1643. doi:10.1093/bioinformatics/btaa1016
862 70. Loftus BJ, Fung E, Roncaglia P, Rowley D, Amedeo P, Bruno D, et al. The genome of the
863 basidiomycetous yeast and human pathogen *Cryptococcus neoformans*. Science. 2005;307: 1321–
864 1324. doi:10.1126/science.1103773
865 71. Love MI, Huber W, Anders S. Moderated estimation of fold change and dispersion for RNA-seq data
866 with DESeq2. Genome Biol. 2014;15: 550. doi:10.1186/s13059-014-0550-8

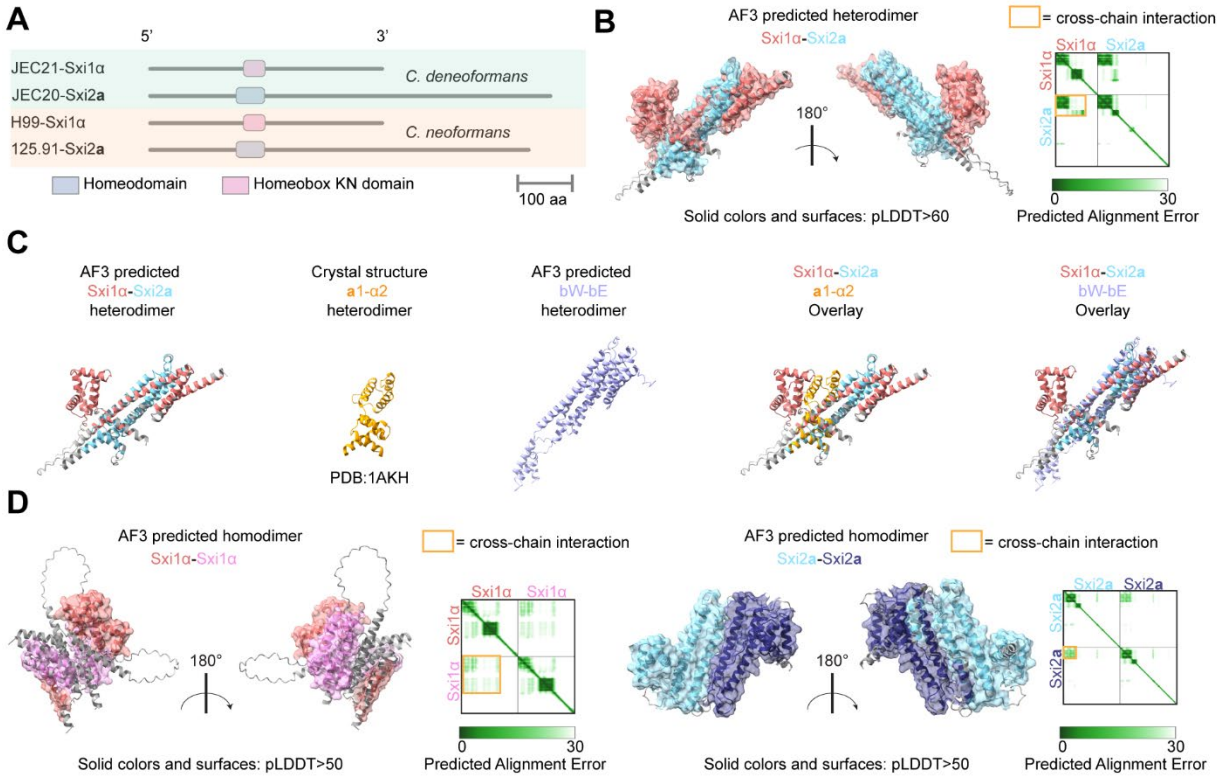

Figure 1. AlphaFold3 predicts heterodimer and homodimers of Sxi1α and Sxi2a.

(A) Predicted domain structures of Sxi1α and Sxi2**a** in *C. neoformans* and *C. deneoformans*. (B) AlphaFold3 (AF3)-predicted heterodimer structure of Sxi1α and Sxi2**a** from *C. deneoformans*. C-terminal disordered regions were hidden for visualization. Only regions with a predicted local distance difference test (pLDDT) score >60 were colored and surfaced. The predicted alignment error (PAE) plot of the predicted Sxi1α-Sxi2**a** heterodimer is displayed in the right panel. (C) Overlay of AlphaFold3-predicted Sxi1α-Sxi2**a** heterodimer with crystal structure of **a**1-α2 (from *S. cerevisiae*, PDB:1AKH) and predicted bW-bE heterodimer (from *U. maydis*, with high confidence ipTM = 0.74 pTM = 0.64). Pairing was performed with the "Matchmaker" function in Chimera X. (D) AlphaFold3-predicted homodimer structures with PAE plots for Sxi1α-Sxi1α (left panel) and Sxi2**a**-Sxi2**a** (right panel). Only regions with a pLDDT score >50 were colored and surfaced.

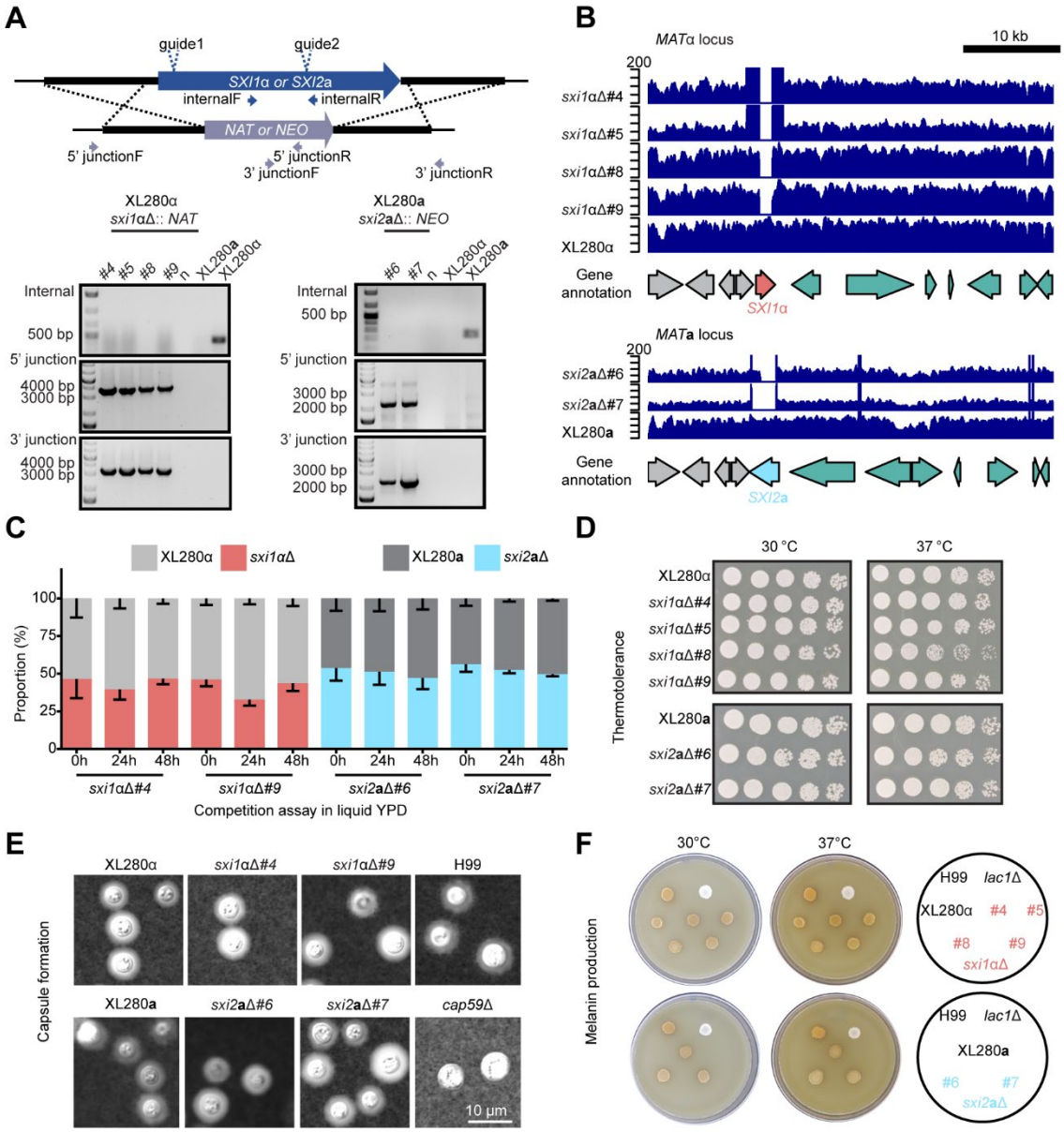

Figure 2. Sxi1α and Sxi2a are not involved in growth, capsule formation, and melanin production. (A) Generation of independent *sxi1*α*Δ* and *sxi2***a***Δ* mutants in XL280α and XL280**a**, respectively. Transformants were verified through internal PCR targeting the ORF, along with 5' and 3' junction PCRs specific to the drug resistance marker to confirm proper integration at the genomic locus. (B) Whole-genome sequencing (WGS) reads mapping confirming the complete or partial deletion of *SXI1*α (red block arrow) and *SXI2***a** (blue block arrow). Genes located within and outside of the mating-type locus are highlighted in green and gray, respectively. (C) *In vitro* competition assays of the *sxi1*α*Δ* and *sxi2***a***Δ* mutants, each carrying either the *NAT* or *NEO* resistance markers, and their corresponding XL280 wildtype strains. Each

889 competition was assayed after 0, 24, 48 hours of incubation, with four independent replicates. Error bars
890 indicate standard deviation. (D) Serial dilutions of *sxi1*α*Δ* and *sxi2***a***Δ* mutants, along with the corresponding
891 XL280 wildtype strains, were spotted on solid YPD media and incubated at 30°C and 37°C. (E) Saturated
892 cultures of the indicated strains, grown in RPMI medium, were stained with India ink to visualize capsule
893 formation. The H99 strain and isogenic *cap59*Δ mutant served as positive and negative controls,
894 respectively. (F) Overnight cultures of the indicated strains were spotted on Niger seed medium to monitor
895 melanin formation. The wildtype H99 strain and isogenic *lac1*Δ mutant served as positive and negative
896 controls, respectively.

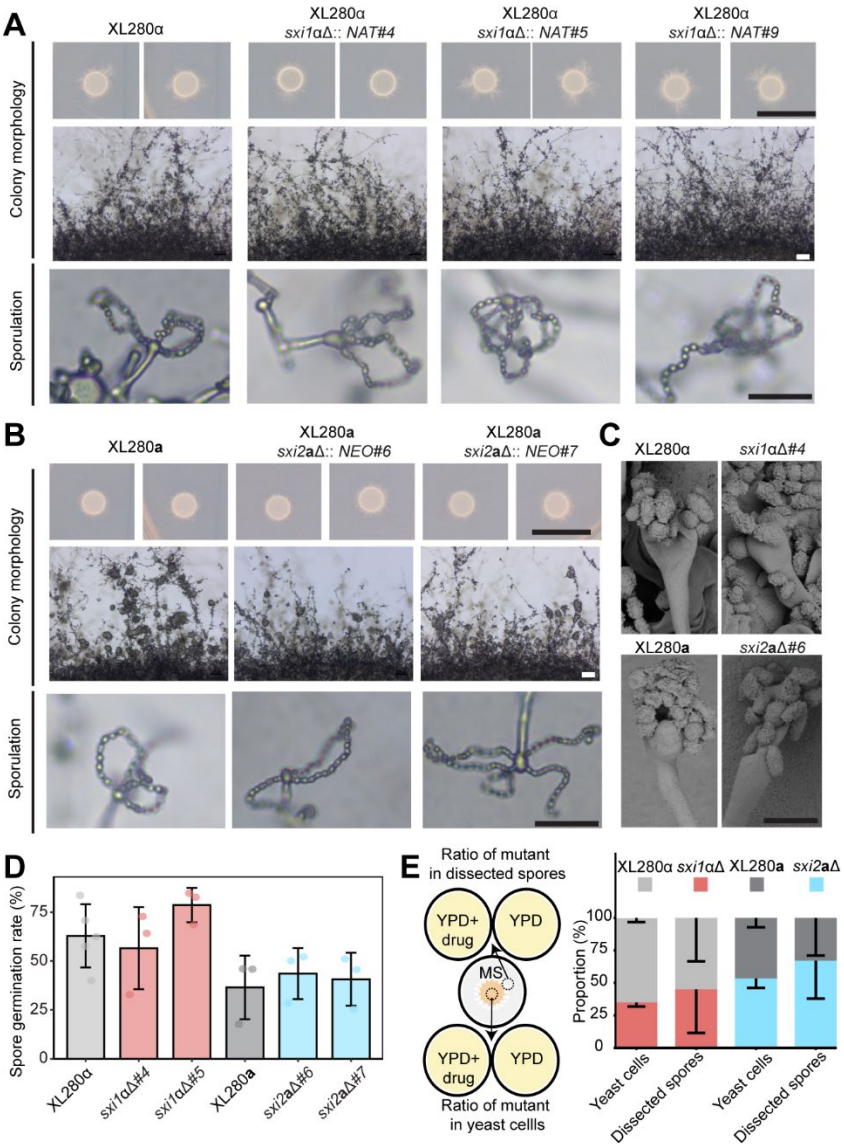

Figure 3. Sxi1α and Sxi2a are not required for hyphal growth or basidium and spore production. (A and B) Colony morphology (top), self-filamentation (middle), and sporulation (bottom) phenotypes of independent *sxi1*αΔ (A) and *sxi2***a**Δ (B) mutants when grown under mating-inducing conditions. Scale bars, 1 cm (upper panel), 100 μm (middle panel) and 20 μm (bottom panel). (C) Scanning electron microscopy (SEM) images of basidia and basidiospores from the indicated solo-culture. Samples were grown on MS media for 1 to 2 weeks before microscopy. Scale bar: 5 μm. (D) Germination rate of random spores dissected from the indicated solo-cultures. At least 3 replicates were performed for each strain (indicated by dots), with error bars depicting standard deviation among replicates. (E) Competition assays of *sxi1*αΔ, *sxi2***a**Δ mutants against their corresponding XL280 wildtype strain. The co-cultures were grown on MS

907 medium under mating-inducing conditions. Spores from the periphery, and yeast cells from the center, of
908 the co-culture spots were dissected and analyzed to determine their origin (i.e., wildtype or mutant), which
909 were then used to infer the relative competitiveness of the mutant strains. Five different co-culture spots
910 were analyzed for each competition.

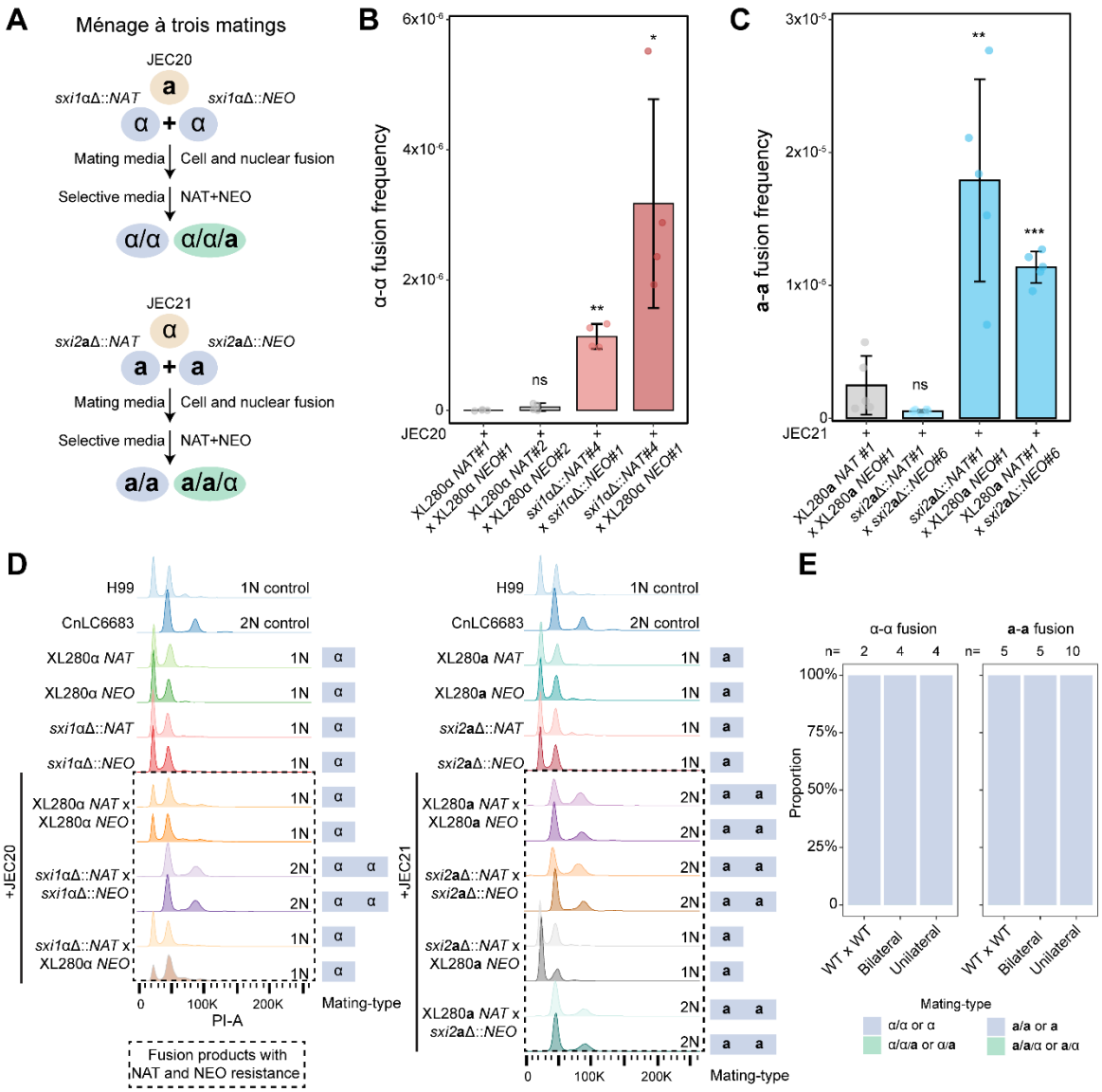

Figure 4. Fusion frequency and ploidy analysis of products from α x α and a x a Ménage à trois matings.

(A) Schematic of the Ménage à trois mating assay. In each mating type background, two strains carrying different selectable markers (NAT or NEO) were co-cultured with a pheromone donor of the opposite mating type to induce cell-cell fusion. NAT and NEO resistant colonies were recovered on selective medium. (B-C) Quantification of α x α (B) and **a** x **a** (C) fusion frequencies for the indicated bilateral and unilateral crosses. Cells from the indicated mating assay on V8 agar (pH = 7.0) for 72 h were plated on YPD + NAT + NEO and YPD to determine the ratio of cell-cell fusion products in the population. Data are presented as mean ± SD from four to five independent biological replicates; each point represents an individual replicate. ns,

921 not significant; * (p-value < 0.05), ** (p-value < 0.01), *** (p-value < 0.001) indicate statistical significance
922 compared to wildtype control. (D) Fluorescence-activated cell sorting (FACS) analysis of DNA content in
923 parental strains and fusion products. H99 (1N control) and CnLC6683 (2N control) originate from the same
924 experiment; their profiles are duplicated in both the left and right panels to facilitate comparison. Fusion
925 products (highlighted by dashed boxes) are annotated with their mating type(s) as determined by
926 genotyping PCR (right). 1N and 2N indicate haploid and diploid DNA content, respectively. (E) Proportion
927 of mating type of fusion products from the indicated crosses.

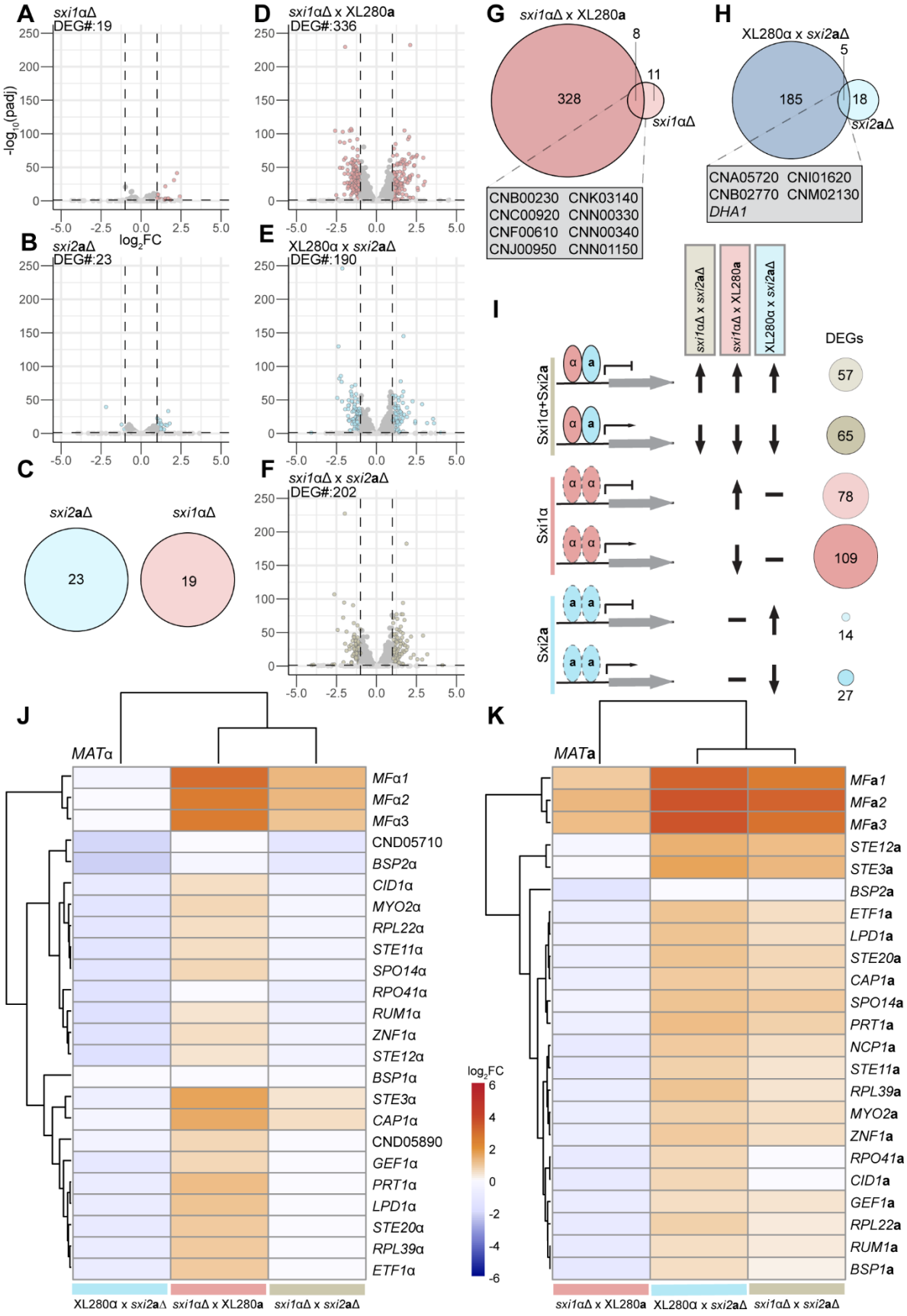
A
sxi1αΔ
DEG#:19
B
sxi2aΔ
DEG#:23
C
sxi2aΔ
sxi1αΔ
23
19
D
sxi1αΔ x XL280a
DEG#:336
E
XL280α x sxi2aΔ
DEG#:190
F
sxi1αΔ x sxi2aΔ
DEG#:202
-log10(padj)
log2FC
G
sxi1αΔ x XL280a
328
8
11
sxi1αΔ
CNB00230 CNK03140
CNC00920 CNN00330
CNF00610 CNN00340
CNJ00950 CNN01150
H
XL280α x sxi2aΔ
185
5
18
sxi2aΔ
CNA05720 CNI01620
CNB02770 CNM02130
DHA1
I
sxi1αΔ x sxi2aΔ
sxi1αΔ x XL280a
XL280α x sxi2aΔ
DEGs
Sxi1α+Sxi2a
Sxi1α
Sxi2a
57
65
78
109
14
27
J
MATα
MFα1
MFα2
MFα3
CND05710
BSP2α
CID1α
MYO2α
RPL22α
STE11α
SPO14α
RPO41α
RUM1α
ZNF1α
STE12α
BSP1α
STE3α
CAP1α
CND05890
GEF1α
PRT1α
LPD1α
STE20α
RPL39α
ETF1α
log2FC
XL280α x sxi2aΔ
sxi1αΔ x XL280a
sxi1αΔ x sxi2aΔ
K
MATa
MFa1
MFa2
MFa3
STE12a
STE3a
BSP2a
ETF1a
LPD1a
STE20a
CAP1a
SPO14a
PRT1a
NCP1a
STE11a
RPL39a
MYO2a
ZNF1a
RPO41a
CID1a
GEF1a
RPL22a
RUM1a
BSP1a
sxi1αΔ x XL280a
XL280α x sxi2aΔ
sxi1αΔ x sxi2aΔ

928

929 **Figure 5. Sxi1 and Sxi2 regulate transcription of distinct subsets of genes during unisexual and**
930 **bisexual reproduction.**
931 (A and B) Differentially expressed genes in *sxi1*αΔ (A) and *sxi2***a**Δ (B) relative to wild-type XL280α or
932 XL280**a**, respectively, during solo cultures (72h at RT on V8 medium). Dashed lines indicate p_{adj} = 0.05 and
933 $\log_2$FC = ± 1. (C) Comparison of DEGs in (A) and (B). (D-F) DEGs relative to XL280α x XL280**a** in crosses
934 between *sxi1*αΔ x XL280**a** (D), XL280α x *sxi2***a**Δ (E), and *sxi1*αΔ x *sxi2***a**Δ (F). (G and H) Comparisons of
935 DEGs in *sxi1*αΔ (G) and *sxi2***a**Δ (H) mutants between solo cultures and α x **a** crosses, with overlapping
936 genes highlighted in the boxes. (I) Schematic of 3 hypotheses for Sxi1α and Sxi2**a** function during α x **a**
937 sexual reproduction. Genes in the first scenario are either positively or negatively regulated by the Sxi1α-
938 Sxi2**a** heterodimer and undergo similar expression changes in all crosses lacking functional Sxi1α and/or
939 Sxi2**a**. Genes in the second scenario are regulated by Sxi1α and are differentially expressed in crosses
940 lacking a functional copy of Sxi1α but not in the XL280α x *sxi2***a**Δ cross because expression changes are
941 independent of Sxi2**a**. Genes in the third scenario are differentially expressed in crosses lacking functional
942 Sxi2**a** (XL280α x *sxi2***a**Δ and *sxi1*αΔ x *sxi2***a**Δ) but unchanged in the presence of a functional copy of Sxi2**a**
943 (*sxi1*αΔ x XL280**a**). (J and K) $\log_2$FC expression values of *MAT*α (J) and *MAT***a** (K) genes in *sxi1*αΔ x
944 XL280**a**, XL280α x *sxi2***a**Δ, and *sxi1*αΔ x *sxi2***a**Δ mutant crosses relative to XL280α x XL280**a** wildtype cross.

945 **Supporting information captions**

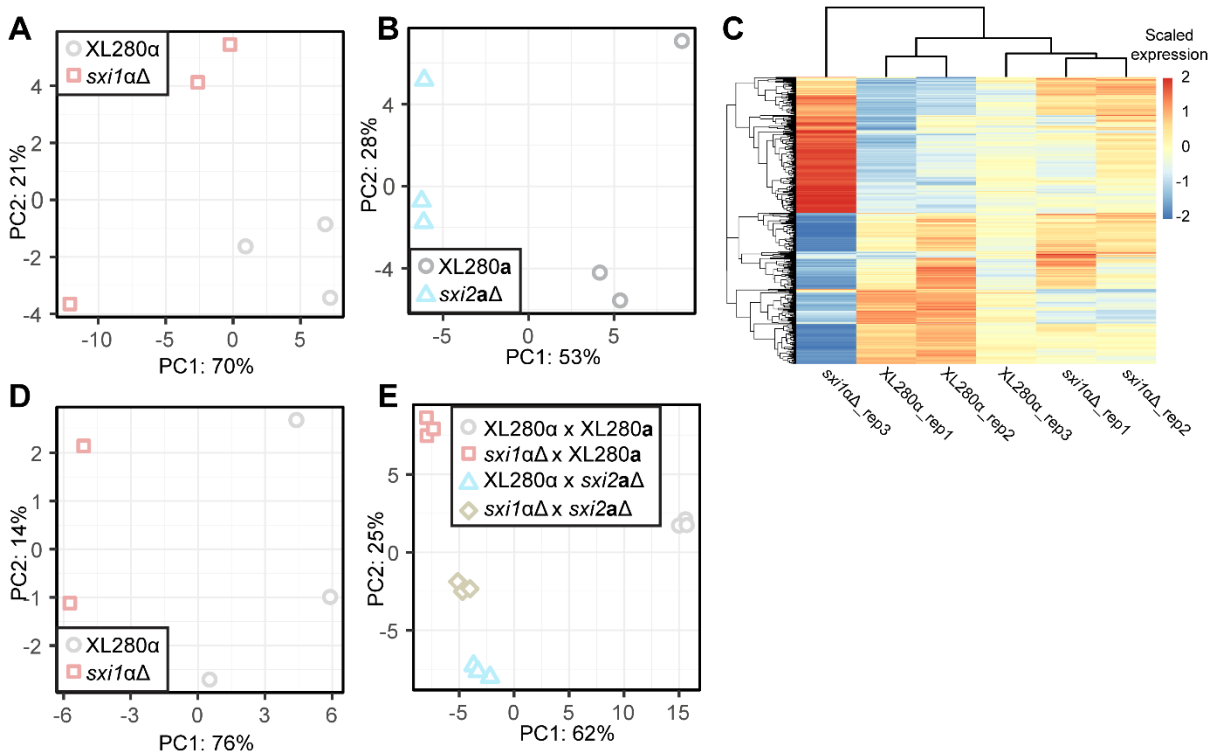

946

947 **Supplemental Figure 1. RNA-seq exploratory data analysis.**

948 All analyses were performed with the top 500 most variable transcripts in each data set. (A and B) PCA of
949 the top 500 most variable transcripts in XL280α (A) and XL280**a** (B) solo-cultures. (C) Hierarchical clustering
950 by sample (x) and transcript (y) of scaled vst-normalized expression values in XL280α and *sxi1*αΔ solo-
951 cultures. (D) PCA of XL280α unisexual crosses excluding *sxi1*αΔ rep 3. (E) PCA of co-culture crosses.

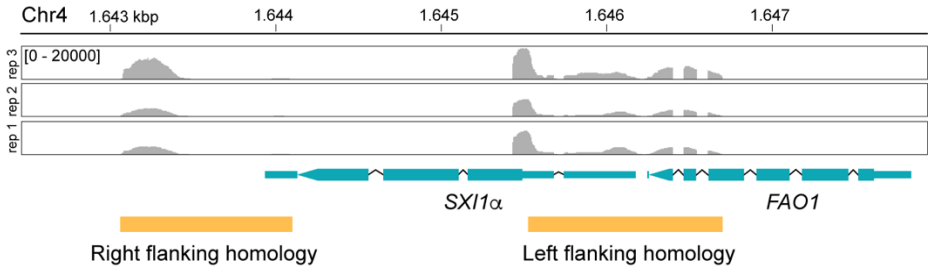

952

953 **Supplemental Figure 2.** RNA-seq reads from XL280α$^{sxi1\Delta}$ unisexual cross mapped to the Sxi1α locus in

954 the XL280α genome. Yellow boxes indicate regions used as homology for the gene deletion cassette.

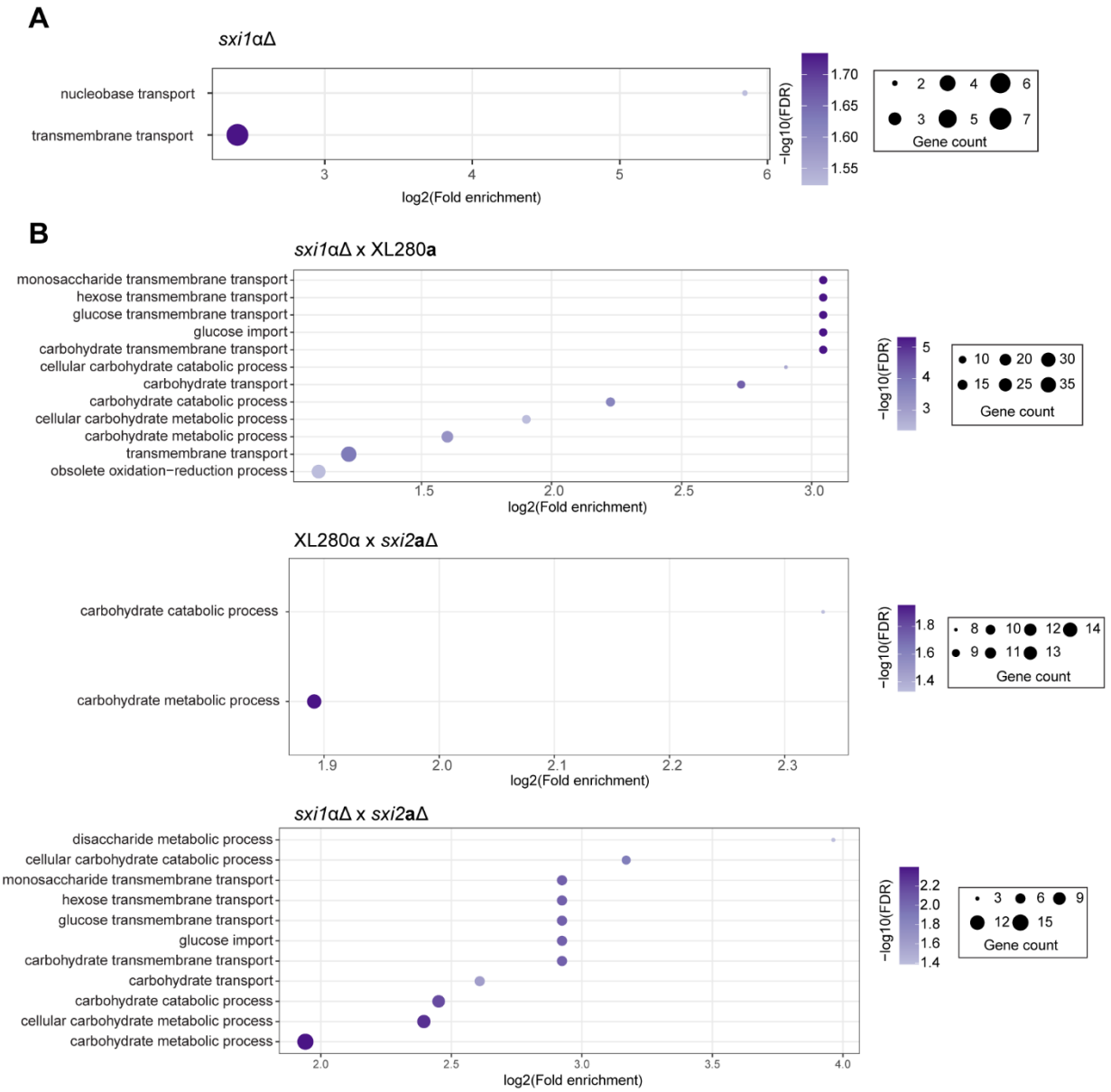

Supplemental Figure 3. GO term enrichment analysis of DEGs from solo- and co-culture crosses. (A) Enriched GO terms in the *sxi1*αΔ solo culture. (B) Enriched GO terms in unilateral (*sxi1*αΔ x XL280**a**, XL280α x *sxi2***a**Δ) and bilateral (*sxi1*αΔ x *sxi2***a**Δ) co-culture mating crosses. Dot size represents the number of DEGs associated with each GO term, and dot color indicates statistical significance as $-\log_{10}$(FDR). GO terms are ranked by $\log_2$(fold enrichment) relative to the whole genome background.

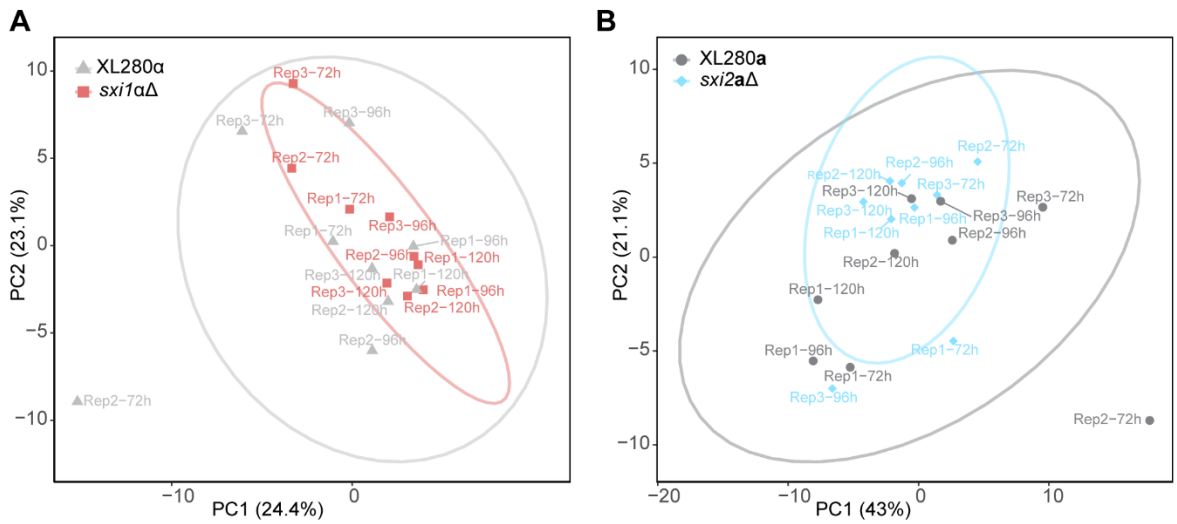

Supplemental Figure 4. Principal component analysis (PCA) of Biolog YT phenotypic microarray data for wildtype and mutant strains.

PCA plots show global metabolic activity profiles based on normalized signal values from Biolog YT plates containing 94 carbon sources, measured at 72, 96, and 120 h. (A) *sxi1*αΔ compared to XL280α. PC1 explains 24.4% of the variance, and PC2 explains 23.1%. (B) *sxi2***a**Δ compared to XL280**a**. PC1 explains 43% of the variance, and PC2 explains 21.1%. Each point represents an individual biological replicate, colored by strain, with ellipses indicating the 95% confidence intervals for each group.

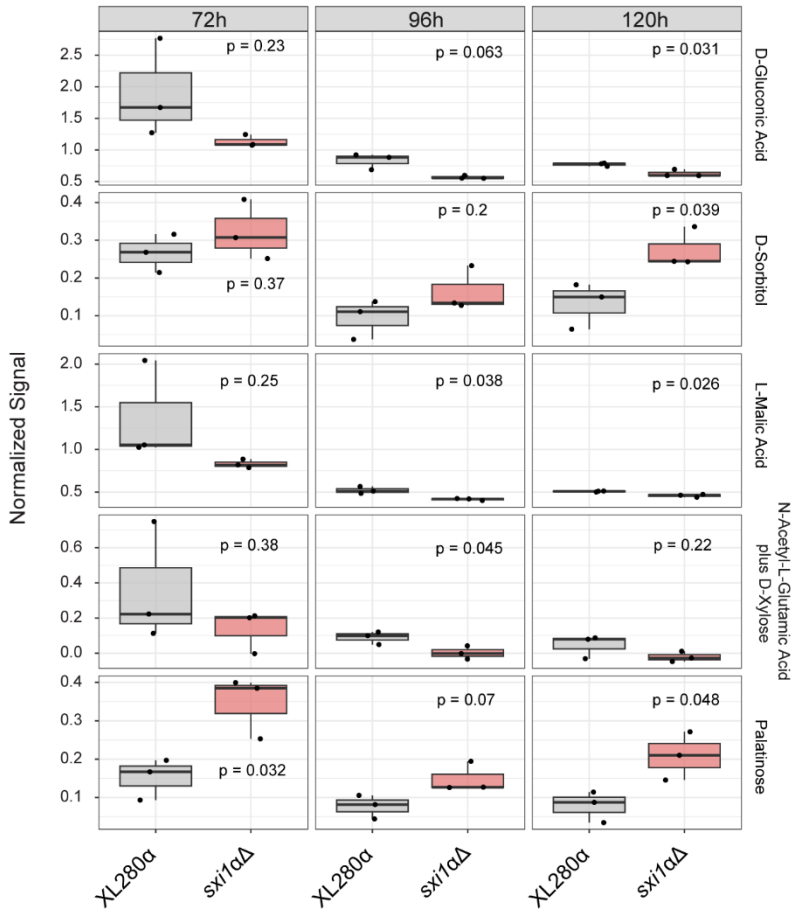

969

970 **Supplemental Figure 5. Carbon sources showing significant differences in utilization between**

971 **sxi1αΔ and XL280α in Biolog YT phenotypic microarrays.**

972 Boxplots display normalized signal values for D-gluconic acid, D-sorbitol, L-malic acid, N-acetyl-L-glutamic

973 acid plus D-xylose, and palatinose at 72, 96, and 120 h. Gray boxes represent XL280α and red boxes

974 represent *sxi1*αΔ. p-values were determined by pairwise t-tests comparing mutant and wild type for each

975 substrate at each time point.

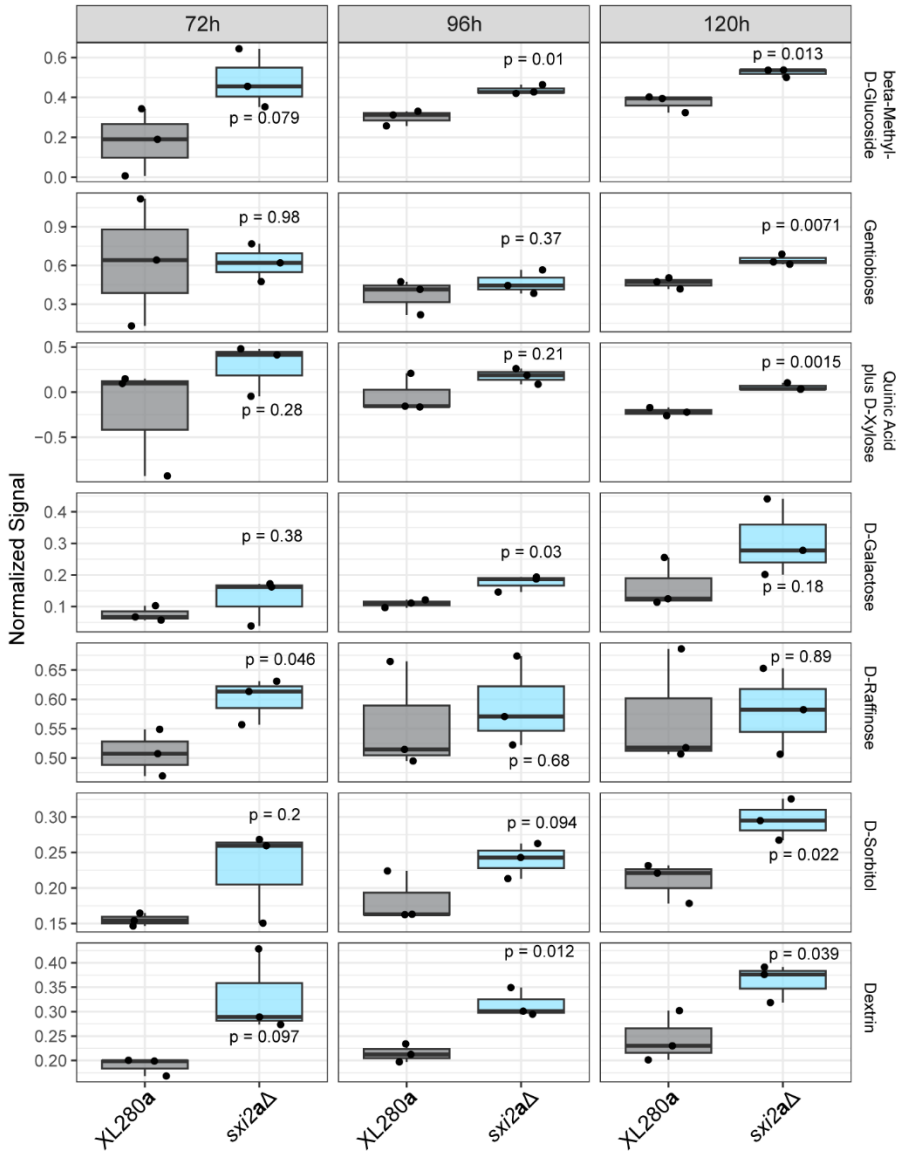

Supplemental Figure 6. Carbon sources showing significant differences in utilization between *sxi2*aΔ** and XL280a in Biolog YT phenotypic microarrays.**

Boxplots display normalized signal values for β-methyl-D-glucoside, gentibiose, quinic acid plus D-xylose, D-galactose, D-raffinose, D-sorbitol, and dextrin at 72, 96, and 120 h. Gray boxes represent XL280**a** and blue boxes represent *sxi2***a**Δ. p-values were determined by pairwise t-tests comparing mutant and wildtype for each substrate at each time point.

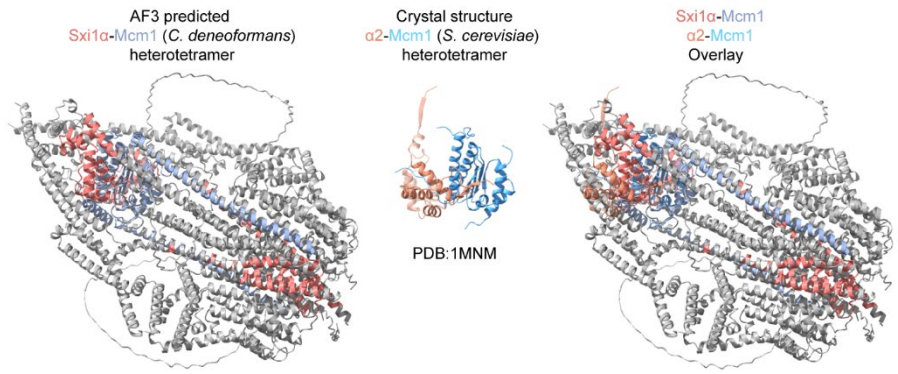

Supplemental Figure 7. Structural comparison of *C. deneoformans* Sxi1α-Mcm1 and *S. cerevisiae* α2-Mcm1 heterotetramers.

Left panel: AlphaFold3-predicted structure of the Sxi1α-Mcm1 heterotetramer in *C. deneoformans* (Sxi1α in salmon, Mcm1 in slate blue). Only regions with a predicted local distance difference test (pLDDT) score >60 were colored and surfaced. Middle panel: Crystal structure of the α2-Mcm1 heterotetramer from *S. cerevisiae* (PDB: 1MNM; α2 in orange, Mcm1 in blue). Right panel: Structural overlay of the AF3-predicted Sxi1α-Mcm1 with the α2-Mcm1 crystal structure. Alignment by UCSF Chimera's MatchMaker yielded a sequence alignment score of 351.9, with an RMSD of 0.432 Å across 76 pruned atom pairs (0.990 Å across all 81 pairs), indicating strong structural similarity between the two heterotetramers.

993 **Table S1 DEGs identified under different mating comparisons.**

994 **Table S2 DEGs shard between unisexual and α-a sexual reproduction.**

995 **Table S3 Strains used in this study.**

996 **Table S4 Primers used in this study.**